Supporting Information

Monocarboxylate-Driven Structural Growth in Calix[n]arene-Polyoxotitanate Hybrid Systems: Utility in Hydrogen Production from Water

Xin-Xue Yang,[a‡] Wei Dong Yu,[b‡] Xiao-Yi Yi,[*a] Lei-Jiao Li,[c] and Chao Liu,[*a]

[a] Hunan Provincial Key Laboratory of Chemical Power Sources, College of Chemistry and Chemical Engineering, Central South University, Changsha, 410083, P. R. China
[b] Hunan Institute of Nuclear Agricultural Science and Space Breeding, Hunan Academy of Agricultural Science, Changsha 410000, P. R. China.
[c]. Jilin Provincial Science and Technology Innovation Canter of Optical Materials and Chemistry, School of Chemical and Environmental Engineering, Changchun University of Science and Technology, Changchun, Jilin 130022, China

*(Chao Liu) E-mail: chaoliu@csu.edu.cn

1. Experimental section

Materials and Characterization. All reagents were purchased commercially and were not further purified when used. Powder X-ray diffraction (PXRD) analysis were performed on a Rigaku Mini Flex II diffractometer at a 2θ range of 5–50° (5° min^{-1}) with CuKα radiation (λ =1.54056 Å). The solid-state UV/Vis spectra data of the cluster samples were obtained on UV-4000 spectrophotometer. We collected the Fourier transform infrared spectroscopy (FTIR) data (4000-500 cm^{-1}) on a PerkinElmer Spectrum 100 FT-IR Spectrometer. Thermogravimetric analyses (TGA) were performed on a Mettler Toledo TGA/SDTA 851e analyzer in N_2 at a temperature range of 50~800℃ (10℃ min^{-1}). Crystallographic data for this article were obtained on a Bruker Apex II CCD diffractometer with graphite-monochromated MoKa radiation. The structures are solved by direct methods and refined on F^2 by full matrix least-squares using new SHELXL program.[1] All of the non-hydrogen atoms are located from Fourier maps and are refined anisotropically. Due to the rotation disorder of tert-butyl groups in the TBC[8] ligand, in all cases ISOR, DELU, SIMU, DFIX constraints were necessary to achieve convergence. All structures which show weak diffraction at wide angle Despite repeated attempts, the X-ray data collected on Ti_6-TBC[8]-**5** was of poor quality. Readers should then consider the X-ray data as preliminary and the proposed structure of Ti_6-TBC[8]-**5** shown in Figure S5 as a model. CCDC 2019347-2019357 contain the crystallographic information herein. The crystallographic data for the reported clusters are listed in **Table 1**.

Synthesis for complex $[Ti_4(TBC[8])(OOCCH_3)_2(CH_3O)_6(CH_3OH)_2]\cdot 4CH_3OH$ (Ti_4-TBC[8]-1): This cluster was prepared according to the literature we reported previously.[1] CCDC 1988956 contain its crystallographic information. 100 mg crystalline samples of $\{TBC[8](Ti_4O_2)(OOCCH_3)_4\}\cdot 4CH_3CN$ were dissolved in methanol. The resulted solution was transferred to a preheated oven at 120 °C for 1 day. After the oven was cooled to room temperature, a small amount of orange crystals of Ti_4-TBC[8]-**1** were obtained on the lid of the reactor.

Synthesis for complex $[Ti_4(TBC[8])(OOC(CH_3)_3)_2(CH_3O)_6(CH_3OH)_2]\cdot 6CH_3OH$ (Ti_4-TBC[8]-2): A mixture of TBC[8] (42 mg, 0.032 mmol), $Ti(O^iPr)_4$ (200 μL, 0.65 mmol), 100 mg pivalic acid (1.96 mmol), and 5 ml CH_3OH was sealed in a 20 mL vessel and transferred to a preheated oven at 120 °C for 3 days. Red crystals were obtained after cooling to 25 °C in a yield of ~65%.

Synthesis for complex $[Ti_4(\mu_2\text{-}O)_2(TBC[8])(OOCH)_4(DMF)_4]\cdot 3.5DMF$ (Ti_4-TBC[8]-3): A mixture of TBC[8] (42 mg, 0.032 mmol), $Ti(O^iPr)_4$ (200 μL, 0.65 mmol), 200 μL formic acid, and 5 ml DMF was

sealed in a 20 mL vessel and transferred to a preheated oven at 80 °C for 3 days. Deep red crystals were obtained after standing at room temperature for one day (yield: ~55%).

Synthesis for complex $[Ti_4(\mu_2\text{-}O)_2(TBC[8])(OOCCH_2CH_2CH_3)_4(DMF)_4]\cdot 4DMF$ (Ti_4-TBC[8]-4): TBC[8] (42 mg, 0.032 mmol) and 200 μL butyric acid were added in a reaction vessel with 5 ml DMF. $Ti(O^iPr)_4$ (200 μL, 0.65 mmol) was added dropwise. The resulting mixtures were then transferred to a preheated oven at 80 °C for 3 days. Red crystals were obtained after cooling to 25 °C (yield: ~65%).

Synthesis for complex $[Ti_4(TBC[8](OOCC_6H_4Br)_4(^iPrO)_4(CH_3CN)_2]\cdot 6CH_3CN$ (Ti_4-TBC[8]-5): TBC[8] (42 mg, 0.032 mmol) and bromobenzoic acid (100 mg, 0.5 mmol) were added in a reaction vessel with 5 ml acetonitrile. $Ti(O^iPr)_4$ (200 μL, 0.65 mmol) was added dropwise. The resulting mixtures were then transferred to a preheated oven at 80 °C for 3 days. Deep red crystals were obtained after cooling to 25 °C (yield: ~35%).

Synthesis for complex $[Ti_6(\mu_3\text{-}O)_2(TBC[8])(OOCC_6H_5)_4(^iPrO)_6]$ (Ti_6-TBC[8]-1): A mixture of TBC[8] (42 mg, 0.032 mmol), $Ti(O^iPr)_4$ (200 μL, 0.65 mmol), 61 mg benzoic acid(0.5 mmol), and 5 ml isopropanol was sealed in a 20 mL vessel and transferred to a preheated oven at 80 °C for 3 days. Red crystals were obtained after cooling to 25 °C (yield: ~75%).

Synthesis for complex $[Ti_6(\mu_3\text{-}O)_2(TBC[8])(OOCC_5H_4N)_4(^iPrO)_6(CH_3O)_2]\cdot 2CH_3CN$ (Ti_6-TBC[8]-2): TBC[8] (42 mg, 0.032 mmol) and 62 mg isonicotinic acid (0.5 mmol) were added in a reaction vessel with 5 ml acetonitrile. $Ti(O^iPr)_4$ (200 μL, 0.65 mmol) was added dropwise. The resulting mixtures were then transferred to a preheated oven at 100 °C for 3 days. A small amount of red crystals of **Ti_6-TBC[8]-2** and colorless crystals were obtained after cooling to 25 °C (yield, about 45% in total with regard to $Ti(OiPr)_4$).

Synthesis for complex $[Ti_6(\mu_3\text{-}O)_2(TBC[8])(OOCC_4H_3O)_4(CH_3O)_2(^iPrO)_6]$ (Ti_6-TBC[8]-3): A mixture of TBC[8] (42 mg, 0.032 mmol), $Ti(O^iPr)_4$ (200 μL, 0.65 mmol), 56 mg furancarboxylic acid (0.5 mmol), and 5 ml isopropanol was sealed in a 20 mL vessel and transferred to a preheated oven at 80 °C for 3 days. Red crystals were obtained after cooling to 25 °C (yield: ~35%).

Synthesis for complex $[Ti_6(\mu_3\text{-}OH)_2(TBC[8])(OOC(CH_3)_3)_9(^iPrO)_5]\cdot {}^i PrOH\cdot$($Ti_6$-TBC[8]-4): TBC[8] (42 mg, 0.032 mmol) and 100 mg pivalic acid 100 mg pivalic acid (1.96 mmol) were added in a reaction vessel with 5 ml acetonitrile. $Ti(O^iPr)_4$ (200 μL, 0.65 mmol) was added dropwise. The resulting mixtures were then transferred to a preheated oven at 100 °C for 3 days. Deep red crystals were obtained (yield: ~65%).

Synthesis for complex $[Ti_6(\mu_3\text{-}O)_2(TBC[8])(OOC(CH_3)_3)_8(^iPrO)_4][Ti_6(\mu_3\text{-}O)_2(\mu_2\text{-}O)_2(OOC(CH_3)_3)_6(^iPrO)_8]$ (Ti_6-TBC[8]-5): 100mg (0.053 mmol) crystalline samples of Ti_6-TBC[8]-4 were dissolved in 2 ml methanol. 3 ml isopropanol was added to the solution. The resulted solution was transferred to a preheated oven at 120 °C for 1 day. After the oven was cooled to room temperature, a few of orange crystals of Ti_6-TBC[8]-5 were obtained on the bottle wall.

Synthesis for complex $[Ti_{10}(\mu_3\text{-}O)_3(TBC[8])(OOCCH_2Br)_{12}(^iPrO)_6]\cdot 2CH_3CN$ (Ti_{10}-TBC[8]-1): A mixture of TBC[8] (42 mg, 0.032 mmol), $Ti(O^iPr)_4$ (200 μL, 0.65 mmol), 70 mg bromoacetic acid (0.5 mmol), and 5 ml CH_3CN was sealed in a 20 mL vessel and transferred to a preheated oven at 80 °C for 2 days. Deep red crystals were obtained after cooling to 25 °C (yield: ~45%).

Synthesis for complex $[Ti_{10}(\mu_3\text{-}O)_3(TBC[8])(OOCC_6F_5)_{12}(^iPrO)_6]$ (Ti_{10}-TBC[8]-2): A mixture of TBC[8] (42 mg, 0.032 mmol), $Ti(O^iPr)_4$ (200 μL, 0.65 mmol), 106 mg pentafluorobenzoic acid (0.5 mmol), and 5 ml acetonitrile was sealed in a 20 mL vessel and transferred to a preheated oven at 80 °C for 2 days. Deep red crystals were obtained after cooling to 25 °C (yield: ~45%).

Photoelectrochemical measurements were performed on a CHI 660e electrochemical workstation in a standard three-electrode electrochemical cell with a working electrode, a platinum plate as the counter electrode, and a saturated calomel electrode as the reference electrode. These three electrodes were immersed in the 0.2M Na_2SO_4 aqueous solution (pH = 6.6). A 300 W high-pressure xenon lamp with UV cut-off filter was used as a full-wavelength light source, located 20 cm away from the working electrode. The on–off cycling irradiation intervals are 20 s. The working electrode was prepared on fluorinedoped tin oxide (FTO) glass. The colloidal dispersion was obtained by ultrasonic treatment of 5 mg ground crystal sample in 1 ml ethanol for 30 min, and then the dispersion was dropped onto FTO

glass (0.75 cm^2 area). After evaporation under an ambient atmosphere for 2 h, the coating film was obtained and used as the working electrode.

H_2 Production Experiment. Photocatalytic hydrogen production tests were investigated in a closed gas circulation system (Beijing Perfect Light Co. Labsolar-III (AG)). Typically, 50 mg of cluster sample was dispersed in 90 mL of H_2O with 10 mL of triethanolamine as a sacrificial agent, and then 33 μL of 1.0 wt % H_2PtCl_6 was added. A 300 W Xe lamp was used as the UV–vis light source. Light passed through a UV cutoff filter ($\lambda > 420$ nm), and then the filtered light was focused onto the reactor. During irradiation, the headspace gas of the reactor was intermittently sampled every 30 min and H_2 from the headspace gas was monitored by a gas chromatograph (Shimadzu GC9860) equipped with a thermal conductivity detector, a 5A molecular sieve column, and Ar as carrier gas.

DFT calculations. DFT calculations were carried out by Gaussian 09 packages[2]. The geometries of the clusters were fully optimized with PBE0 functional[3]. The initial geometries of the clusters were taken from the corresponding crystal structure data. The "double-ξ" quality basis set LANL2DZ associated with the pseudopotential was employed on atom Ti and Br[4, 5]. The 6-31G(d,p) basis set was employed for nonmetal atoms. The calculated electronic density plots for frontier molecular orbitals were prepared by using the Gaussview 5.0 software. Some related frontier molecular orbitals of Ti_4-TBC[8]-**2** and Ti_4-TBC[8]-**5** are ploted in Figure S56.

References:

1. X. X. Yang, W. D. Yu, X. Y. Yi and C. Liu, Accurate Regulating of Visible-Light Absorption in Polyoxotitanate–Calix[8]arene Systems by Ligand Modification, Inorg. Chem. **2020**, *56*, 7512-7519.

2. M. J. Frisch, G. W. Trucks, H. B. Schlegel, G. E. Scuseria, M. A. Robb, J. R. Cheeseman, G. Scalmani, V. Barone, B. Mennucci, G. A. Petersson, H. Nakatsuji, M. Caricato, X. Li, H. P. Hratchian, A. F. Izmaylov, J. Bloino, G. Zheng, J. L. Sonnenberg, M. Hada, M. Ehara, K. Toyota, R. Fukuda, J. Hasegawa, M. Ishida, T. Nakajima, Y. Honda, O. Kitao, H. Nakai, T. Vreven, J. A. Montgomery, J. E. Peralta, F. Ogliaro, M. Bearpark, J. J. Heyd, E. Brothers, K. N. Kudin, V. N. Staroverov, R. Kobayashi, J. Normand, K. Raghavachari, A. Rendell, J. C. Burant, S. S. Iyengar, J. Tomasi, M. Cossi, N. Rega, N. J. Millam, M. Klene, J. E. Knox, J. B. Cross, V. Bakken, C. Adamo, J. Jaramillo, R. Gomperts, R. E. Stratmann, O. Yazyev, A. J. Austin, R. Cammi, C. Pomelli, J. W. Ochterski, R. L. Martin, K. Morokuma, V. G. Zakrzewski, G. A. Voth, P. Salvador, J. J. Dannenberg, S. Dapprich, A. D. Daniels, O. Farkas, J. B. Foresman, J. V. Ortiz, J. Cioslowski and D. J. Fox, Gaussian 09, Revision A.02, Gaussian Inc., Wallingford, CT, 2009.

3. C. Adamo and V. Barone, Toward reliable density functional methods without adjustable parameters: The PBE0 model, *J. Chem. Phys*., **1999**, 110, 6158.

4. P. J. Hay and W. R. Wadt, Ab initio effective core potentials for molecular calculations. Potentials for the transition metal atoms Sc to Hg, *J. Chem. Phys.*, **1985**, 82, 270.

5. P. J. Hay and W. R. Wadt, Ab initio effective core potentials for molecular calculations. Potentials for K to Au including the outermost core orbitals, *J. Chem. Phys*., **1985**, 82, 299.

2. Structure of Compounds

Table S1. X-ray measurements and structure solution of compounds.

Compounds	**Ti_4-TBC[8]-2**	**Ti_4-TBC[8]-3**	**Ti_4-TBC[8]-4**	**Ti_4-TBC[8]-5**	**Ti_6-TBC[8]-1**
CCDC	2019347	2019348	2019349	2019350	2019351
Formula	$C_{112}H_{170}O_{26}Ti_4$	$C_{104}H_{160.5}N_{7.5}O_{22.5}Ti_4$	$C_{140}H_{212}O_{30}N_8Ti_4$	$C_{145}H_{176}O_{20}N_8Ti_4Br_4$	$C_{137}H_{165}O_{26}Ti_6$
T(K)	150	150	150	150	150
F_w	2123.99	1881.22	2535.08	2862.07	2514.96
Crystal system	monoclinic	monoclinic	triclinic	monoclinic	monoclinic
Space group	$P2_1/c$	P21/n	P-1	C2/c	$P2_1/n$
a, Å	14.6214(11)	14.2318(11)	14.4277(6)	26.964(7)	18.124(2)
b, Å	28.2561(17)	14.6532(12)	14.6080(5)	24.087(7)	15.607(2)
c, Å	14.3350(9)	18.0810(15)	17.6599(7)	23.8198(5)	25.066(3)

α/ °	90	103.020(6)	82.875(3)	90	90
β/°	93.955(6)	102.821(6)	72.447(4)	94.280(2)	105.645(3)
γ/°	90	107.509(5)	75.012(4)	90	90
V/Å^3	5908.3(7)	3328.9(5)	3423.7(2)	15427.0(8)	6827.4(15)
Z	2	1	1	4	2
ρ_{calcd}/gcm^{-3})	1.086	0.835	1.185	1.229	1.223
μ/mm^{-1})	0.318	0.277	0.293	1.297	0.401
F(000)	2060	896	1304.0	5938	2654.0
Data/restraints /parameters	9802/58/639	13068/163/730	13423/129/862	15086/183/1020	11617/185/888
Goof	1.001	0.917	1.062	1.068	1.033
R_1/wR_2(I> 2σ(I))	0.1038/0.2251	0.0662/0.1541	0.0649/0.1933	0.0696/0.2038	0.0756/0.1228
R_1/wR_2(all data)	0.1839/ 0.2580	0.1546/ 0.1734	0.0969/0.2115	0.1042/0.2236	0.2189/0.1527

Compounds	**Ti_6-TBC[8]-2**	**Ti_6-TBC[8]-3**	**Ti_6-TBC[8]-4**	**Ti_6-TBC[8]-5**	**Ti_{10}-TBC[8]-1**	**Ti_{10}-TBC[8]-2**
CCDC	2019352	2019353	2019355	2019354	2019356	2019357
T (K)	150	150	150	150	150	150
Formula	$C_{140}N_8O_{26}Ti_6H_{177}$	$C_{128}H_{165}O_{30}Ti_6$	$C_{151}H_{225}O_{34}Ti_6$	$C_{190}H_{300}O_{56}Ti_{12}$	$C_{134}N2H_{164}Br_{12}O_{46}Ti_{10}$	$C_{196}H_{158}O_{46}Ti_{10}F_{60}$
F_w	2675.14	2470.99	2871.70	4039.72	3976.23	4866.20
Crystal system	monoclinic	monoclinic	monoclinic	triclinic	triclinic	triclinic
Space group	$P2_1/n$	$P2_1/n$	$P2_1/n$	P-1	P-1	P-1
a, Å	18.742(2)	17.6540(7)	21.391(2)	15.419(5)	14.9660(2)	17.662(9)
b, Å	15.688(9)	15.3326(5)	25.794(3)	19.356(6)	15.494(3)	18.0164(5)
c, Å	24.515(3)	24.8024(11)	33.0748(4)	20.165(7)	20.8678 (3)	21.2467(9)
α/ °	90	90	90	84.214(19)	98.6889(14)	68.017(3)
β/°	106.320(7)	105.9960(10)	99.423(10)	70.821(18)	110.5977(15)	69.349(5)
γ/°	90	90	90	86.94(2)	100.0332(14)	61.753(4)
V/Å^3	6917.6(5)	6453.6(4)	18002.9(3)	5654(3)	4341.02(13)	5393.7(5)
Z	2	2	4	1	1	1
ρ_{calcd}/gcm^{-3})	1.245	1.272	1.060	1.159	1.490	1.498
μ/mm^{-1})	0.398	0.425	2.654	0.467	7.520	4.090
F(000)	2738	2610	6140.0	2090.0	1926.0	2460
Data/restraints/ parameters	14055/154/918	11864/113/840	32628/249/1937	12006/338/1313	17492/186/1076	18263/362/1730
Goof	1.026	1.035	1.041	0.950	1.022	1.032
R_1/wR_2(I> 2σ(I))	0.0551/0.1394	0.0675/0.1458	0.0655/0.1740	0.1049/0.2497	0.0655/0.1841	0.0953/0.2603
R_1/wR_2(all data)	0.1102/0.1762	0.1107/0.1664	0.0928/0.1915	0.2356/0.2953	0.0833/0.2014	0.1507/0.3050

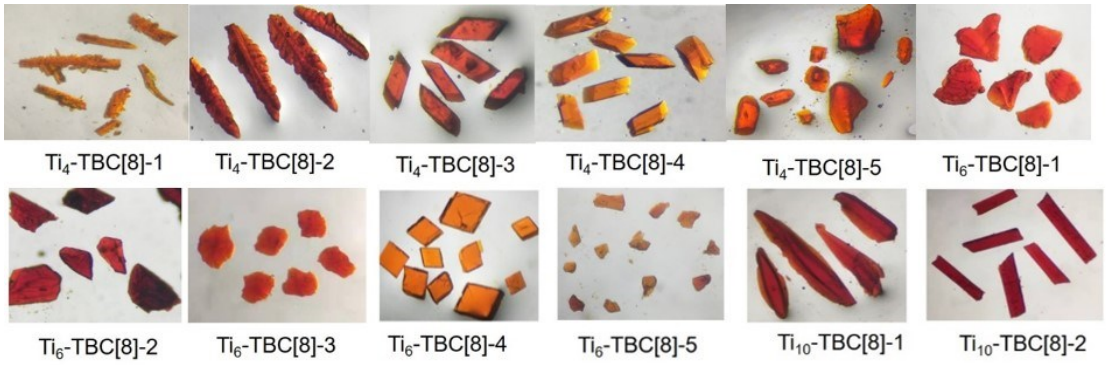

Figure S1. Crystal pictures of the Ti_x-TBC[8] clusters.

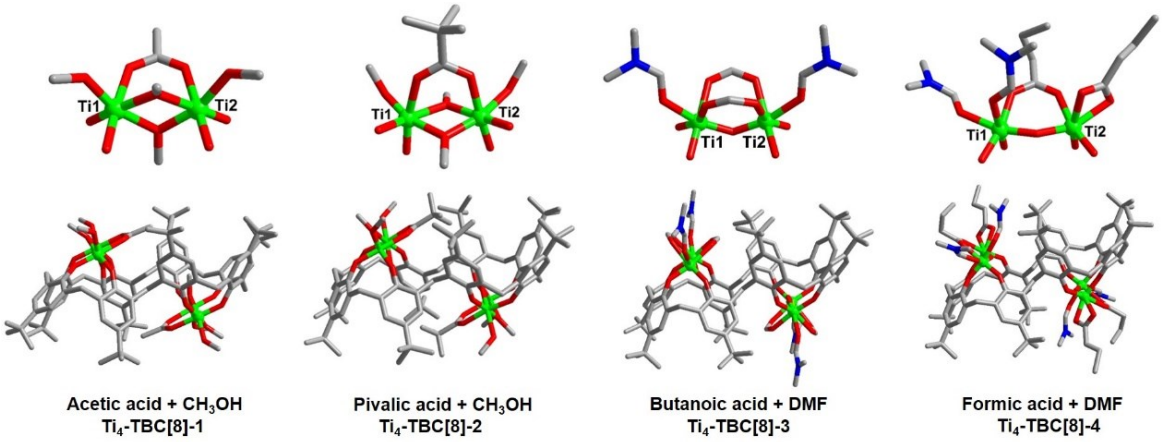

Figure S2. Structure of Ti_4-TBC[8]-**1-4**. Different binding modes of carboxylate groups around the {Ti_2} units were observed.

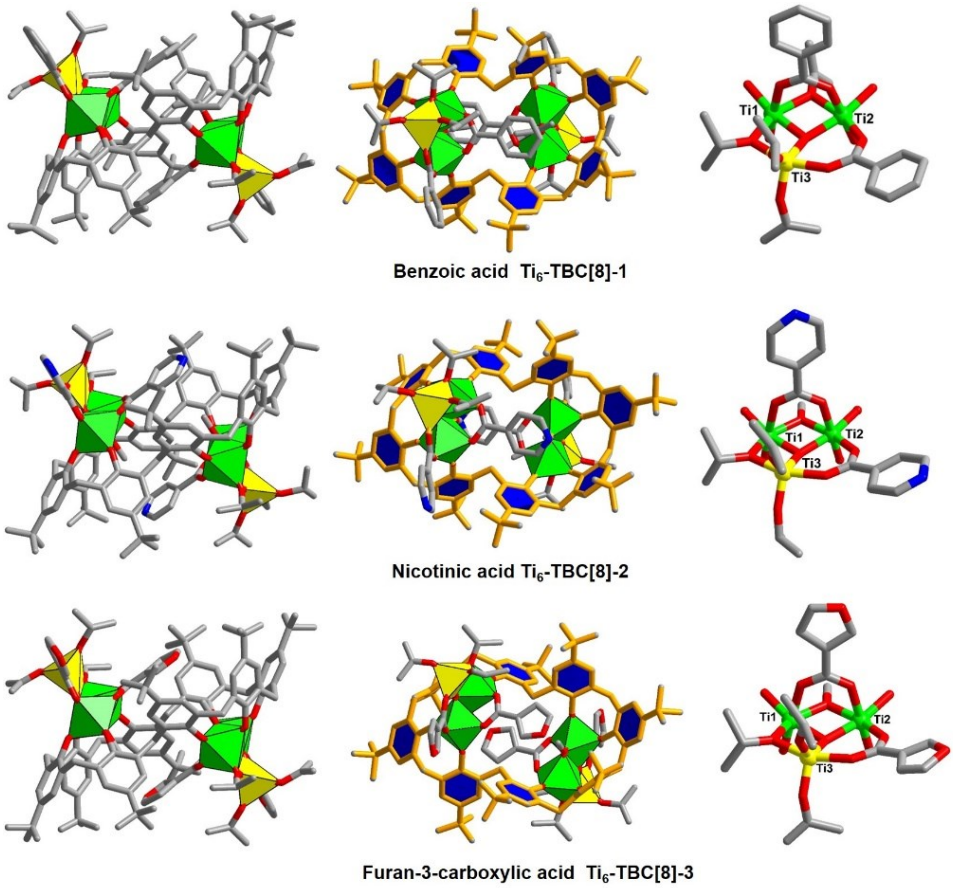

Figure S3. Structure of Ti_6-TBC[8]-**1-3**.

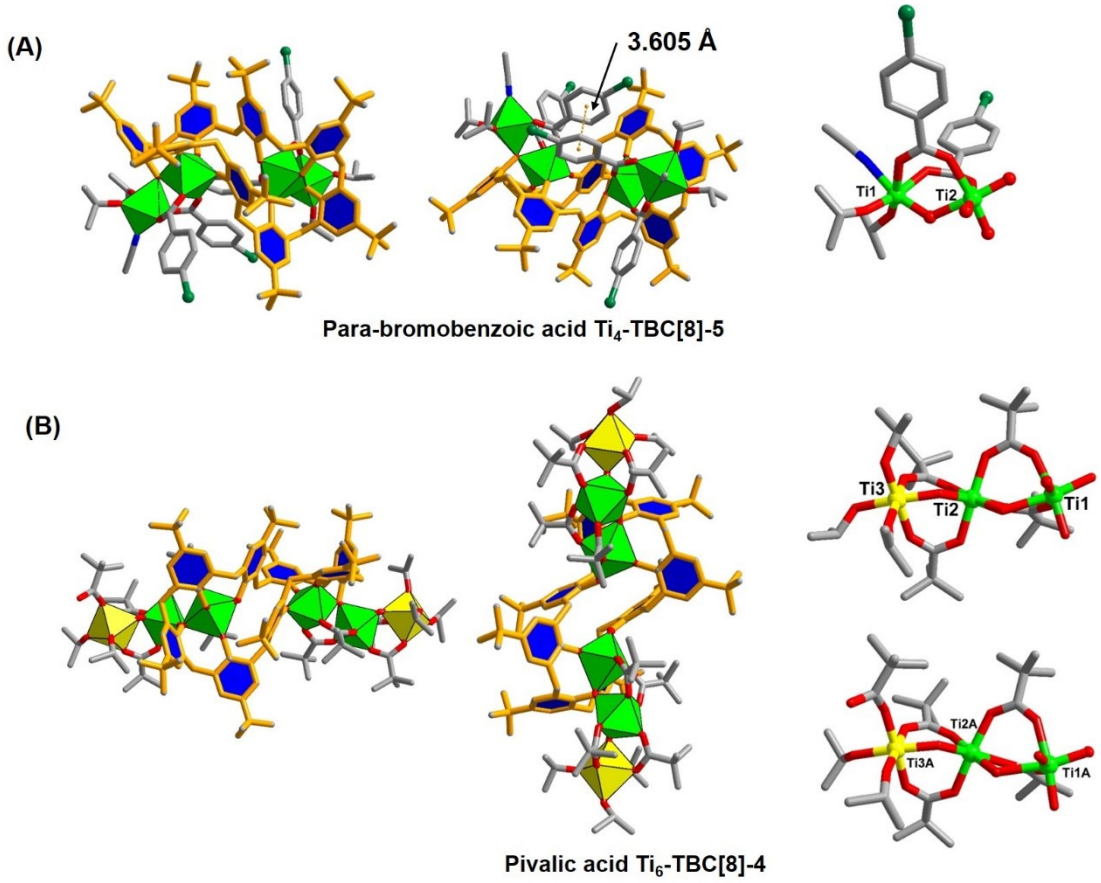

Figure S4. Structure of Ti_4-TBC[8]-**5** and Ti_6-TBC[8]-**4**.

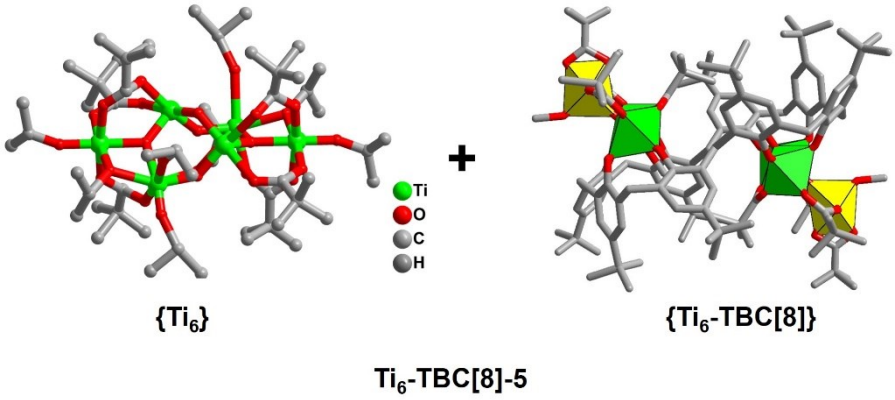

Figure S5. The two sub-structures in the compound Ti_6-TBC[8]-5.

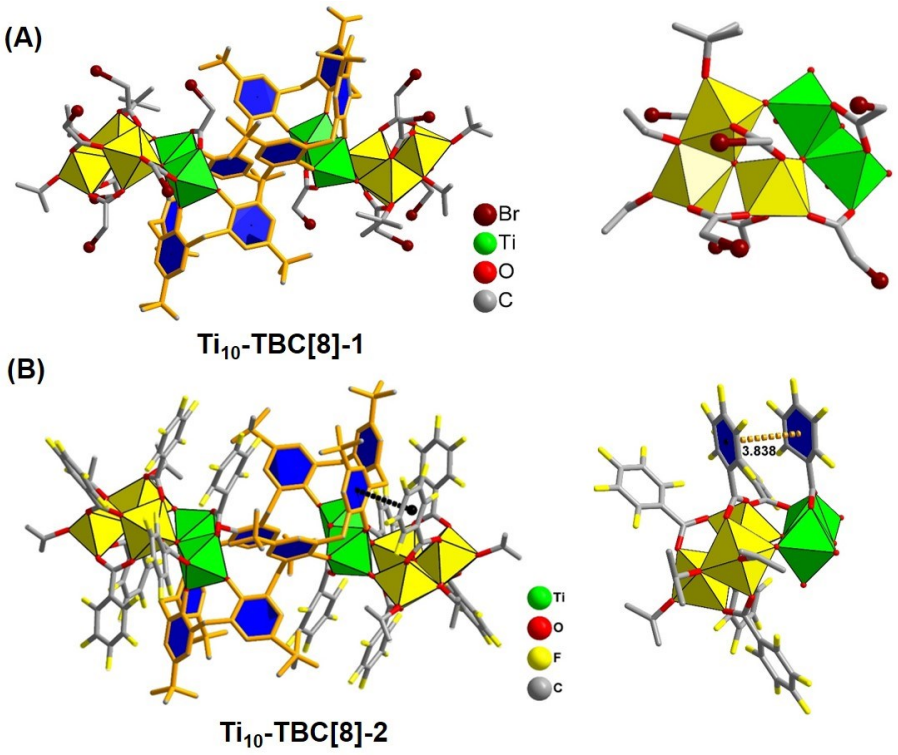

Figure S6. Structure of Ti_{10}-TBC[8]-**1** and Ti_{10}-TBC[8]-**2**.

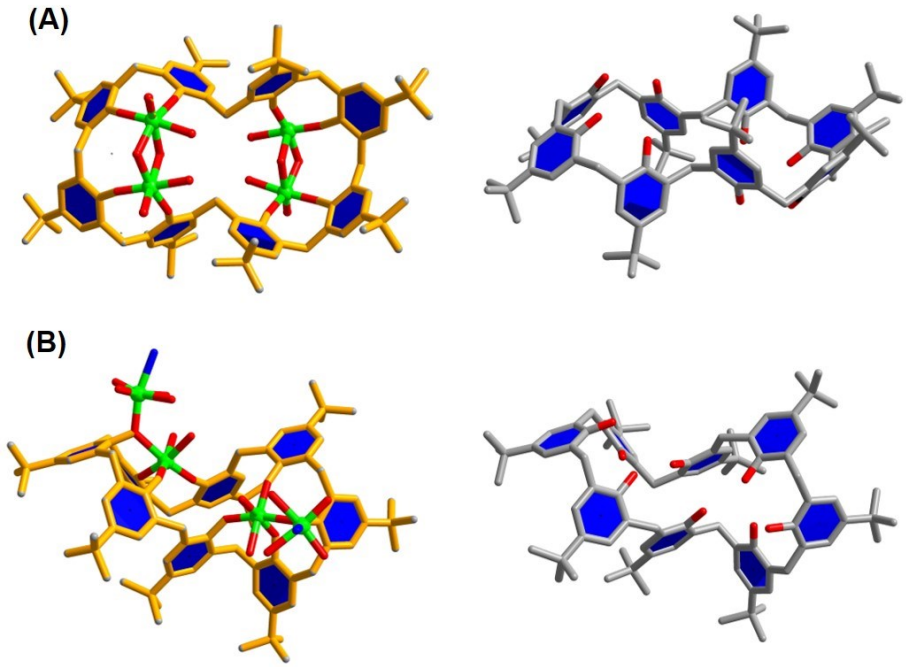

Figure S7. (A) The configuration and coordination mode of the TBC[8] ligand in the structure of Ti_4-TBC[8]-**1-4,** Ti_6-TBC[8]-**1-4** and Ti_{10}-TBC[8]-**1-2;** (B) The configuration and coordination mode of the TBC[8] ligand in the structure of Ti_4-TBC[8]-**5** and Ti_6-TBC[8]-**4.**

2 Powder X-ray diffraction

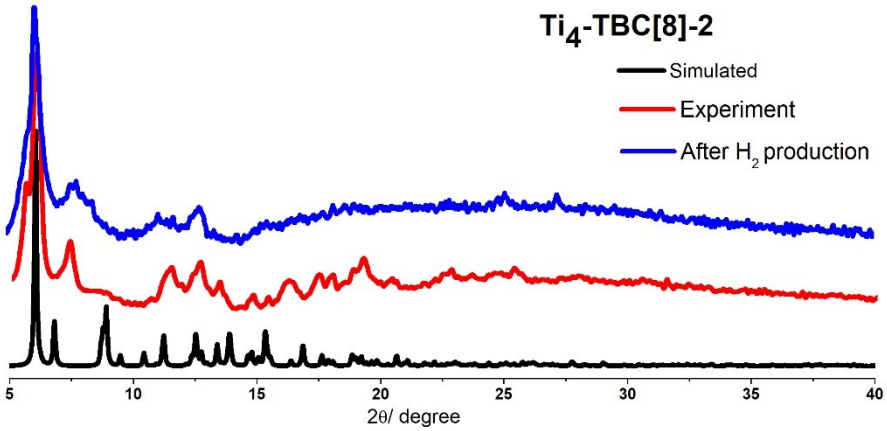

Figure S8. The XRD patterns of TBC[8]-Ti_4-**2** (the simulated pattern, as-synthesized product, sample after photocatalytic water-splitting).

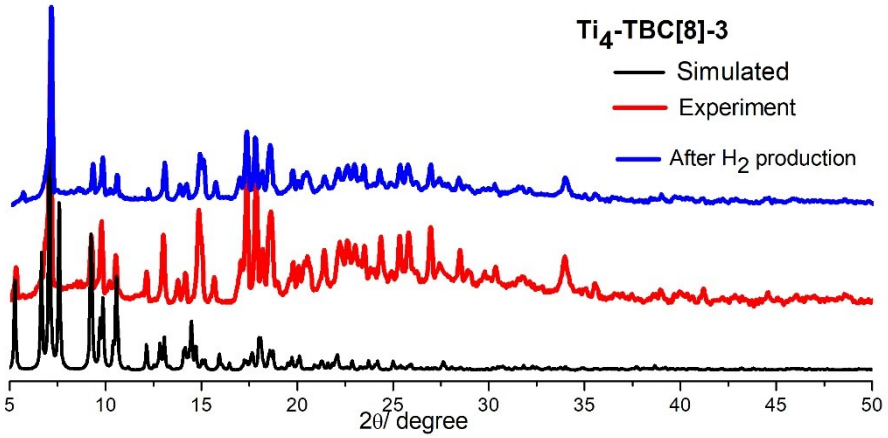

Figure S9. The XRD patterns of TBC[8]-Ti_4-3(the simulated pattern, as-synthesized product, sample after photocatalytic water-splitting).

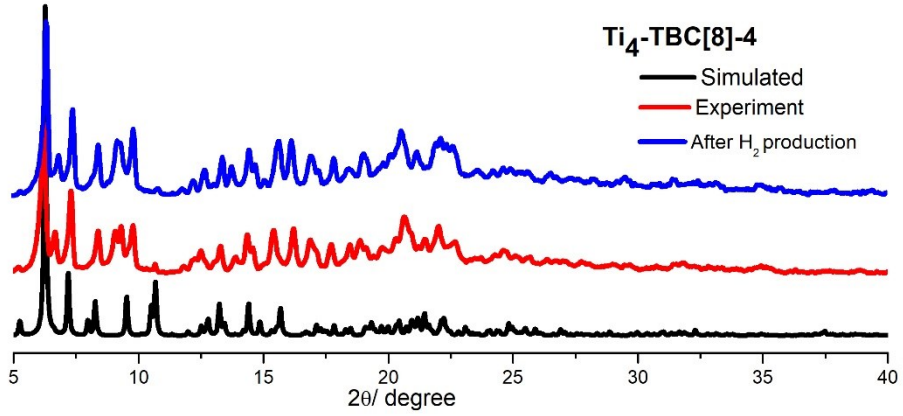

Figure S10. The XRD patterns of Ti_4-TBC[8]-4(the simulated pattern, as-synthesized product, sample after photocatalytic water-splitting)

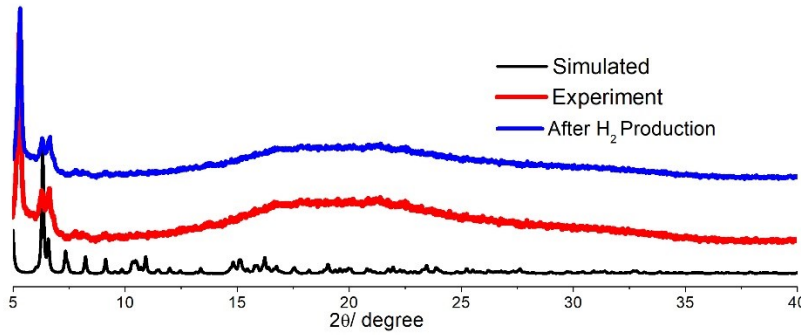

Figure S11. The XRD patterns of Ti_4-TBC[8]-5(the simulated pattern, as-synthesized product, sample after photocatalytic water-splitting)

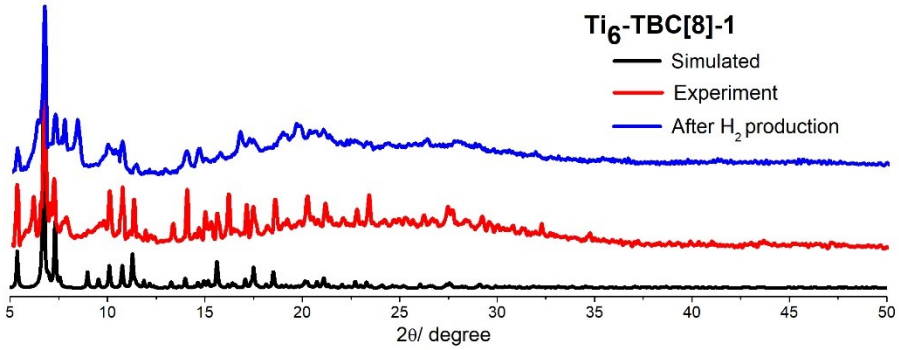

Figure S12. The XRD patterns of Ti_6-TBC[8]-1 (the simulated pattern, as-synthesized product, sample after photocatalytic water-splitting).

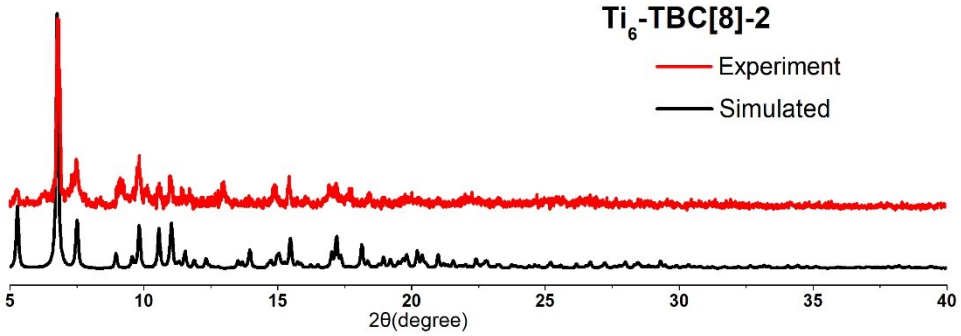

Figure S13. The XRD patterns of Ti_6-TBC[8]-2 (the simulated pattern, as-synthesized product).

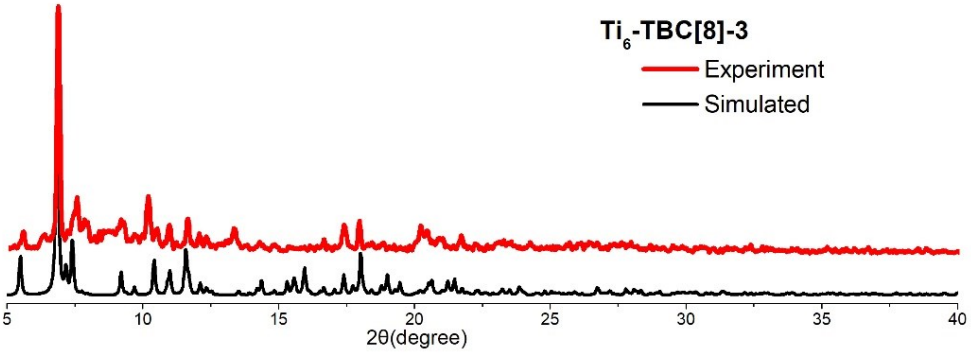

Figure S14. The XRD patterns of Ti_6-TBC[8]-3 (the simulated pattern, as-synthesized product).

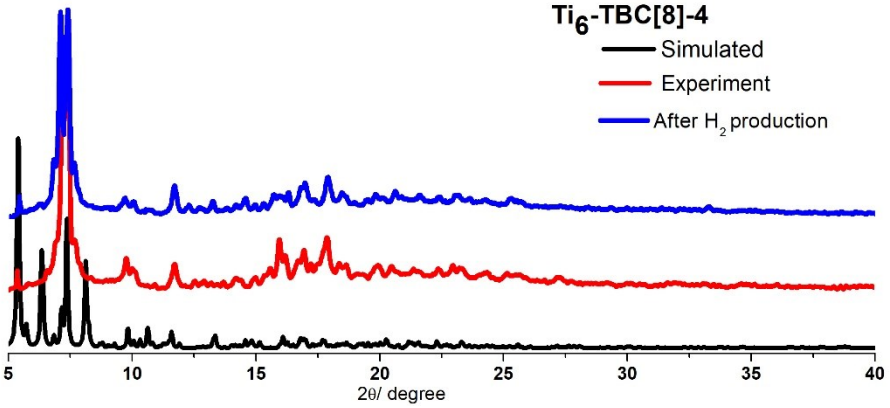

Figure S15. The XRD patterns of Ti_6-TBC[8]-4 (the simulated pattern, as-synthesized product, sample after photocatalytic water-splitting).

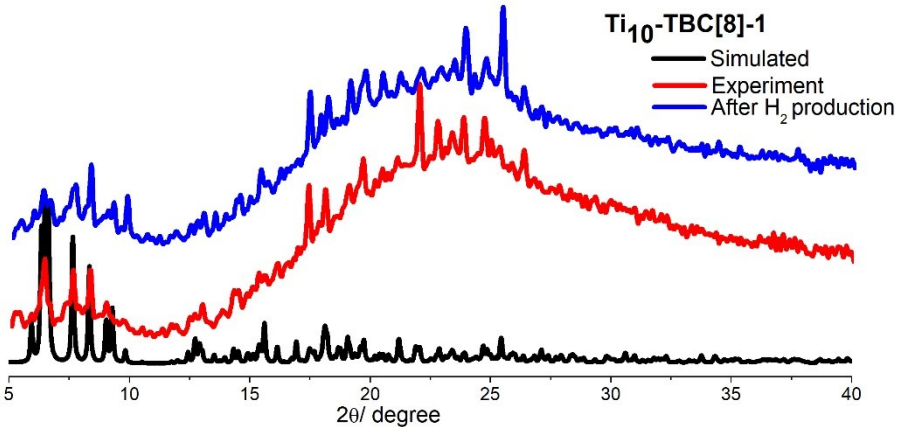

Figure S16. The XRD patterns of Ti_{10}-TBC[8]-1 (the simulated pattern, as-synthesized product, sample after photocatalytic water-splitting.

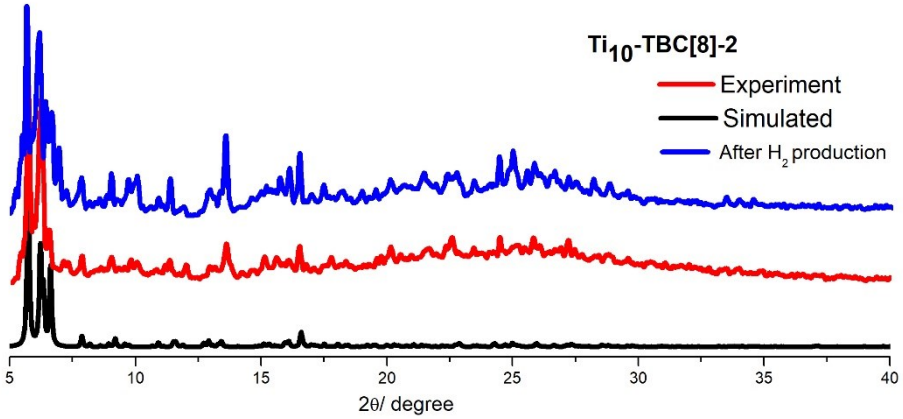

Figure S17. The XRD patterns of Ti_{10}-TBC[8]-2 (the simulated pattern, as-synthesized product, sample after photocatalytic water-splitting.

3 FT-IR spectrum

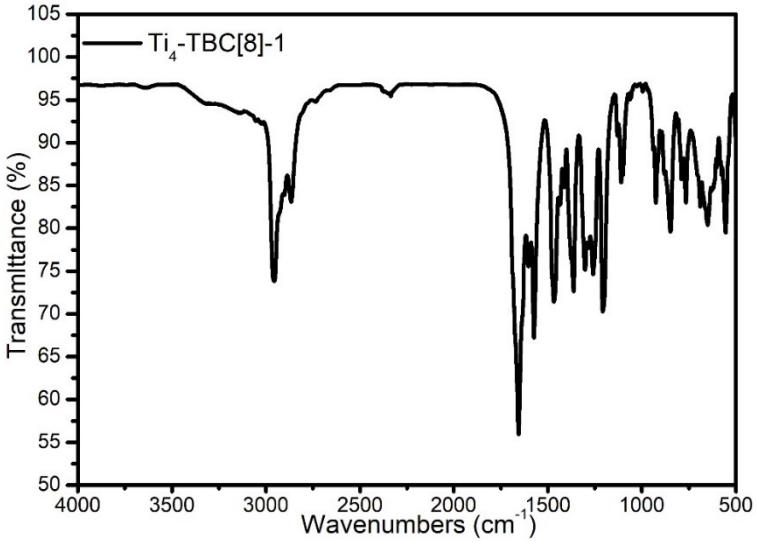

Figure S18. IR spectra of crystal sample of Ti_4-TBC[8]-**2**.

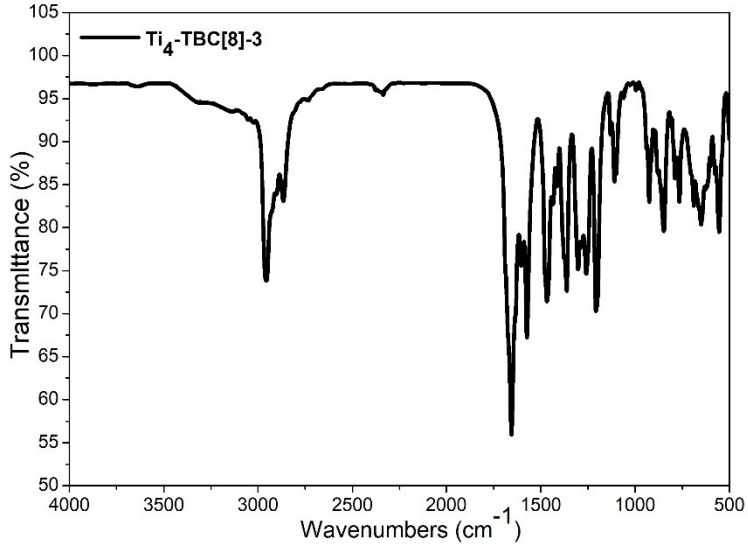

Figure S19. IR spectra of crystal sample of Ti_4-TBC[8]-**3**.

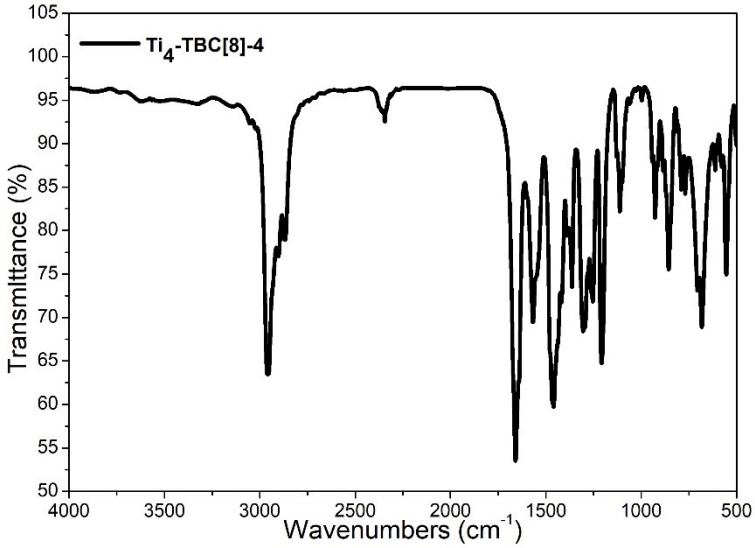

Figure S20. IR spectra of crystal sample of Ti_4-TBC[8]-**4.**

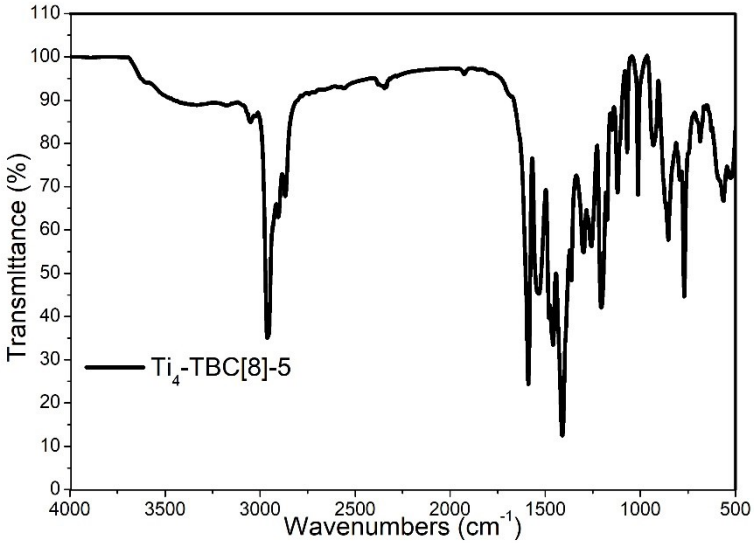

Figure S21. IR spectra of crystal sample of Ti_4-TBC[8]-**5**.

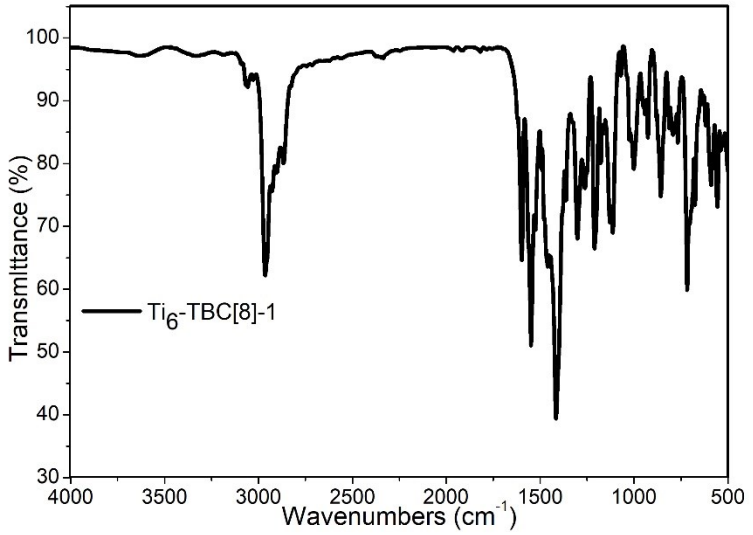

Figure S22. IR spectra of crystal sample of Ti_6-TBC[8]-**1**.

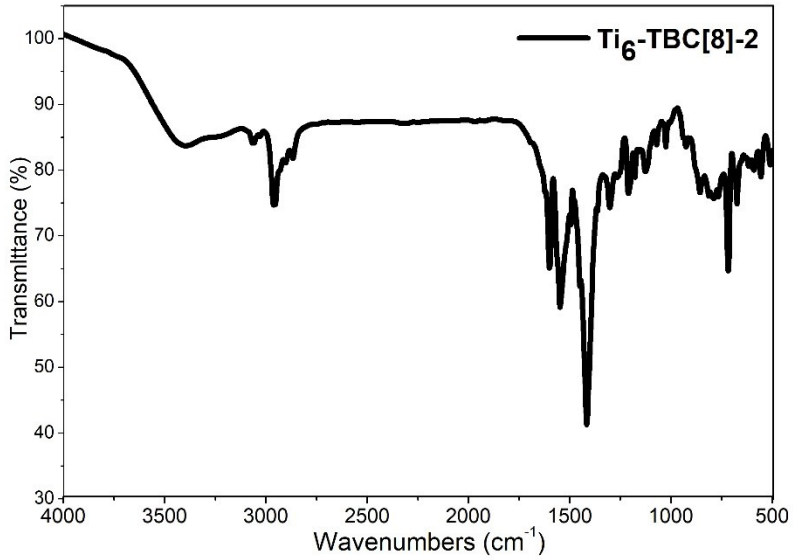

Figure S23. IR spectra of crystal sample of Ti_6-TBC[8]-**2**.

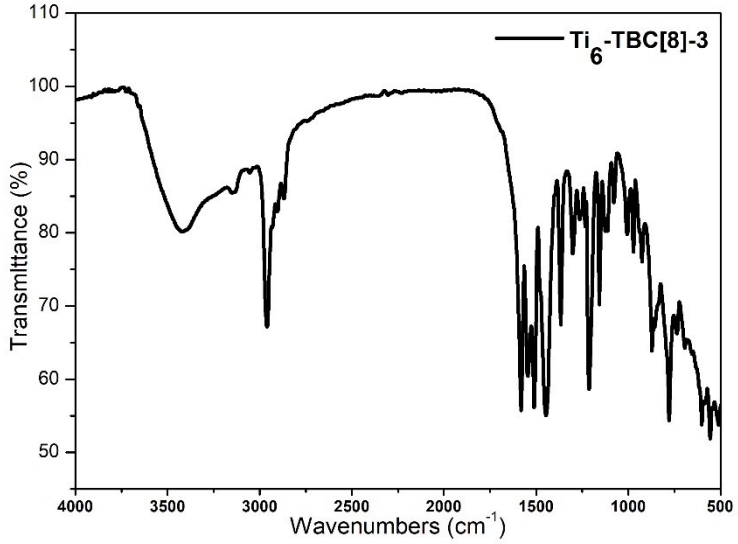

Figure S24. IR spectra of crystal sample of Ti_6-TBC[8]-**3**.

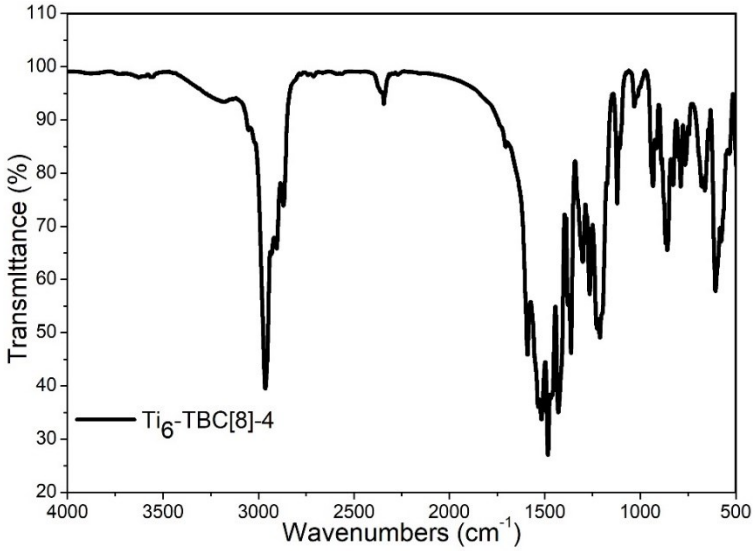

Figure S25. IR spectra of crystal sample of Ti_6-TBC[8]-**4.**

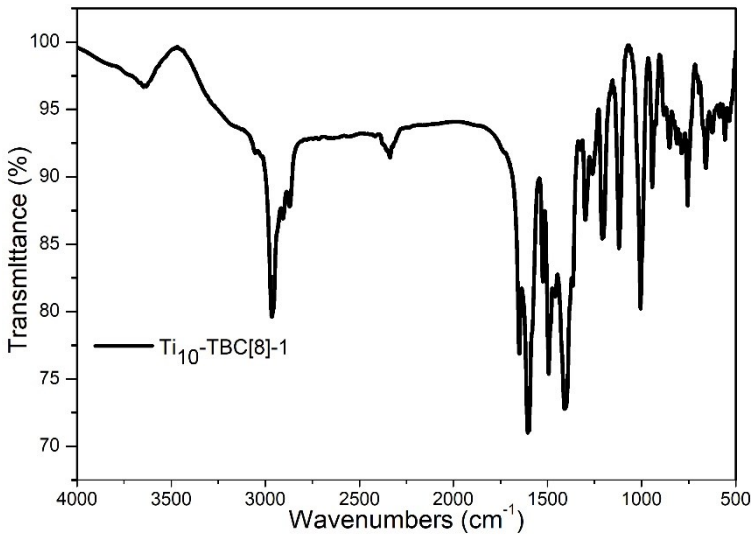

Figure S26. IR spectra of crystal sample of Ti_{10}-TBC[8]-**1**.

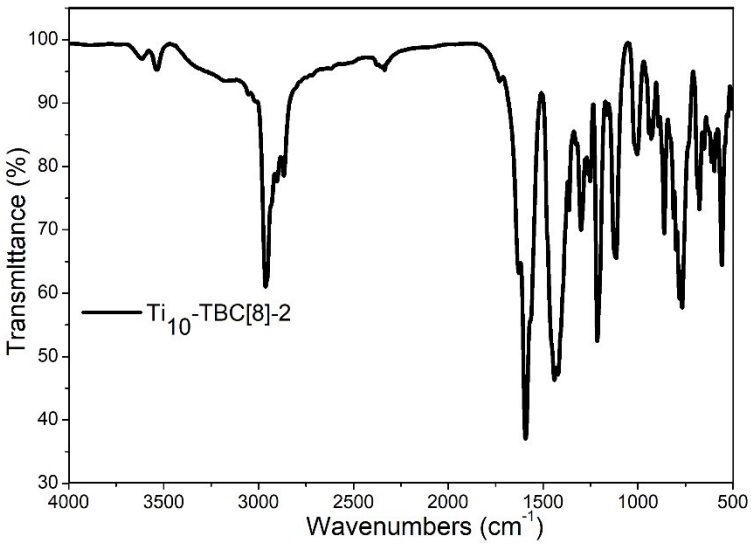

Figure S27. IR spectra of crystal sample of Ti_{10}-TBC[8]-**2**.

4 TG-Measurement

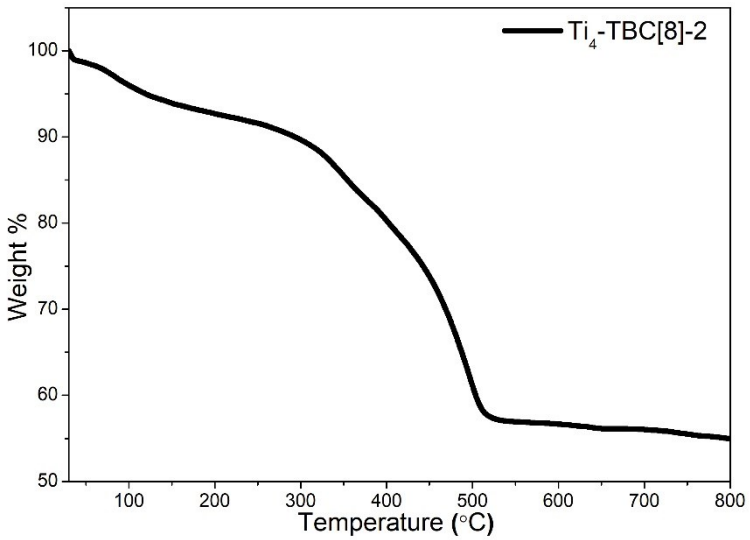

Figure S28. Thermal decomposition curve of Ti_4-TBC[8]-2.

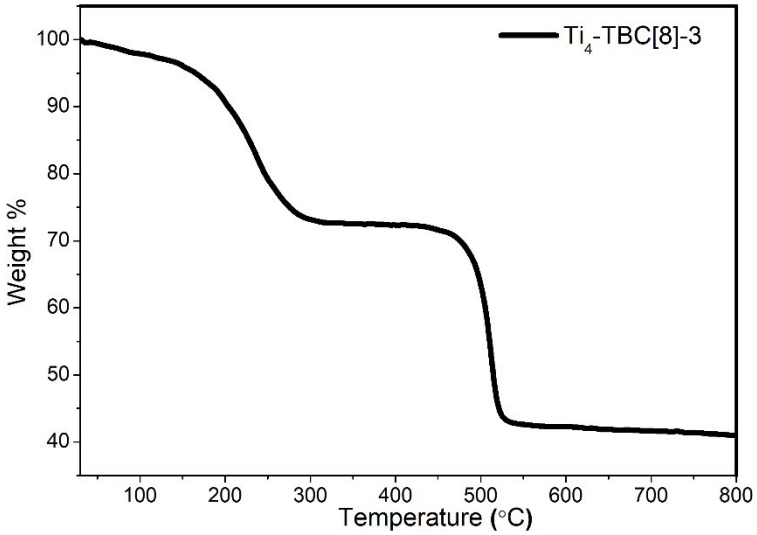

Figure S29. Thermal decomposition curve of Ti_4-TBC[8]-3.

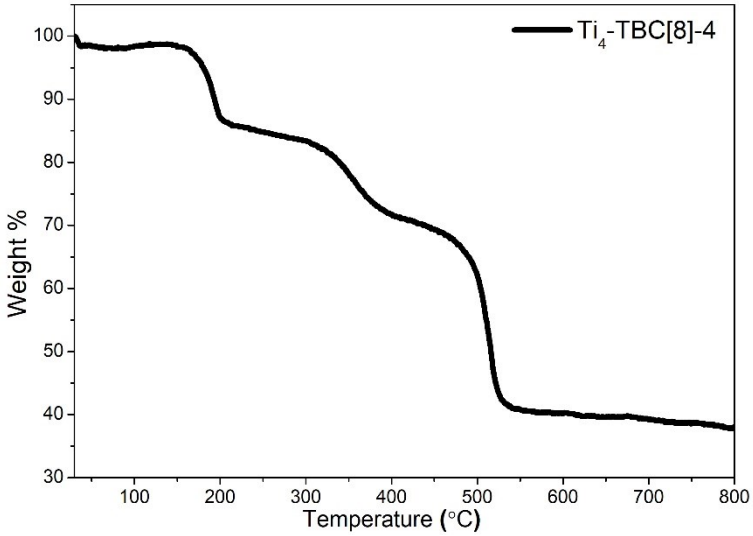

Figure S30. Thermal decomposition curve of Ti_4-TBC[8]-4.

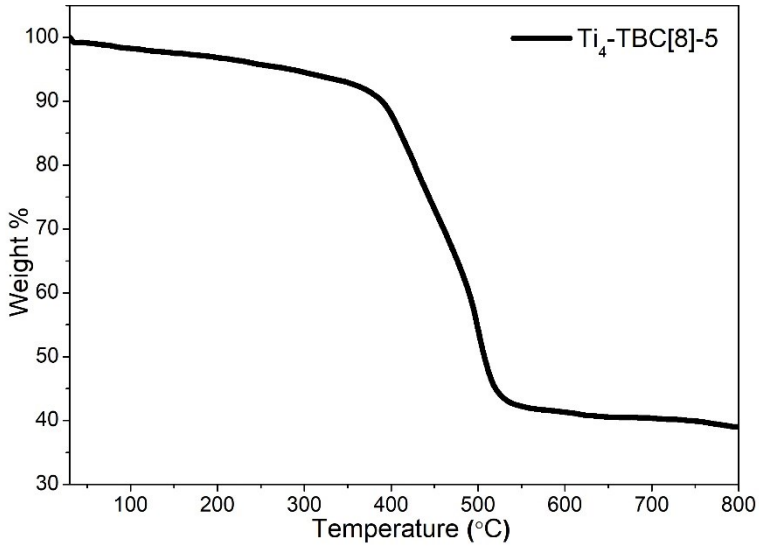

Figure S31. Thermal decomposition curve of Ti_4-TBC[8]-5.

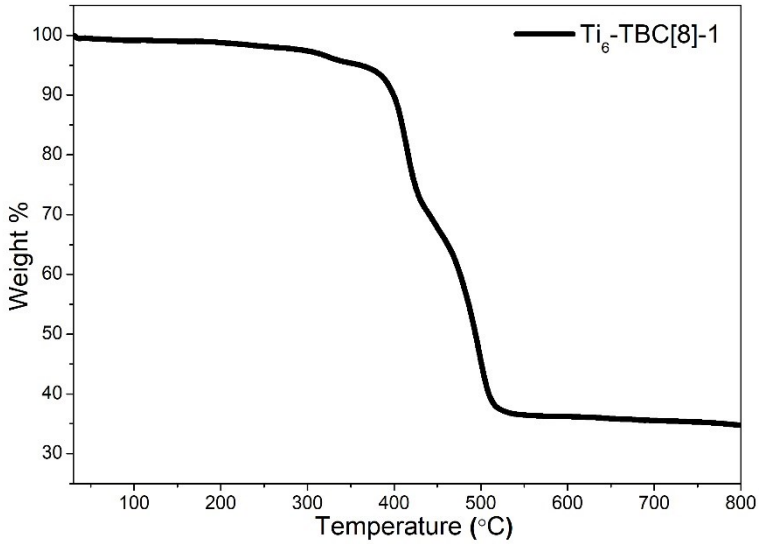

Figure S32. Thermal decomposition curve of Ti_6-TBC[8]-1.

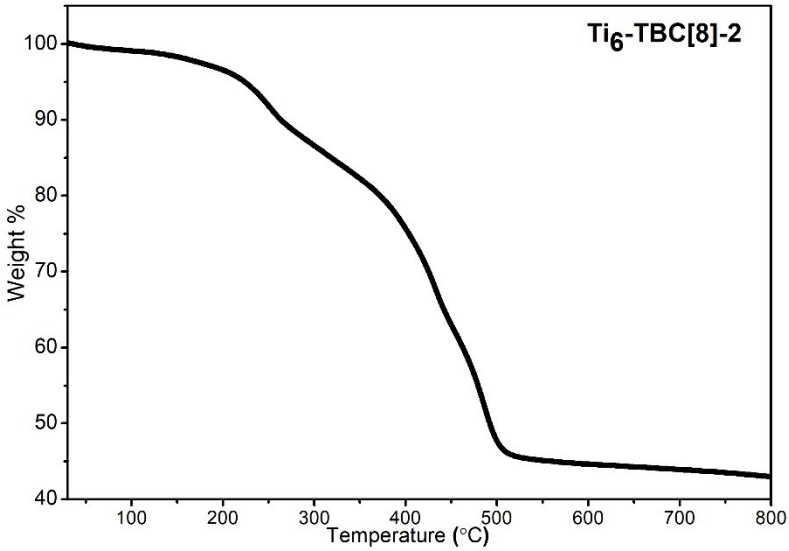

Figure S33. Thermal decomposition curve of Ti_6-TBC[8]-2.

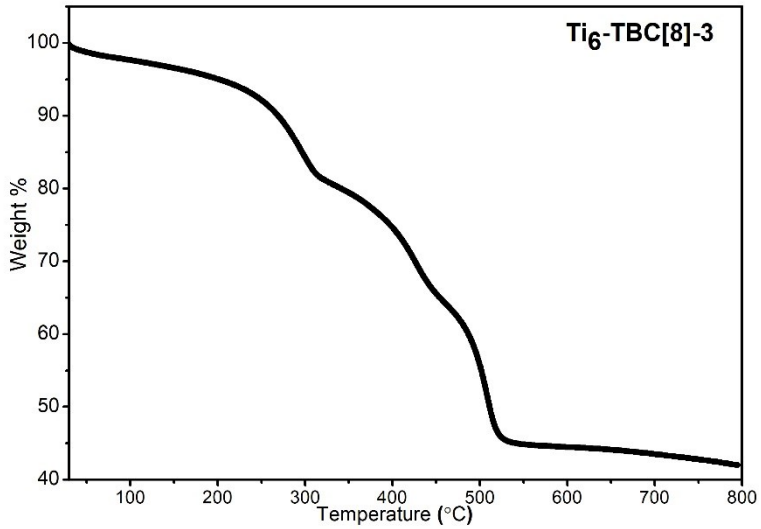

Figure S34 Thermal decomposition curve of Ti_6-TBC[8]-3.

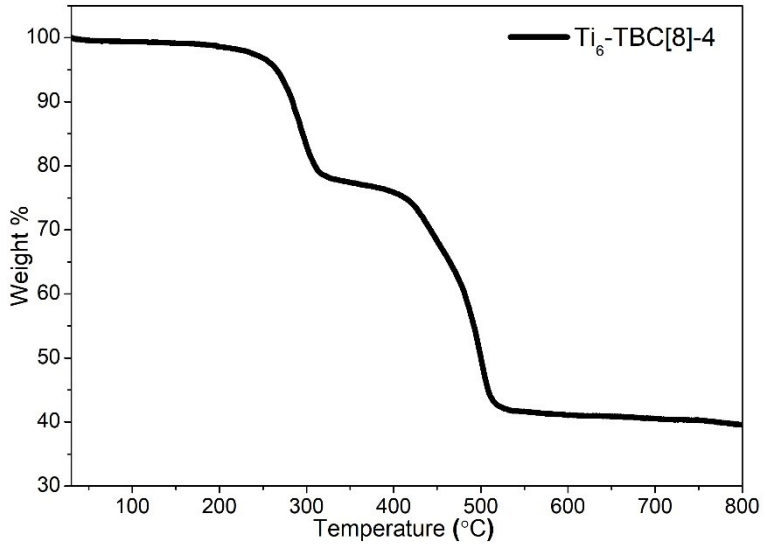

Figure S35 Thermal decomposition curve of Ti_6-TBC[8]-4.

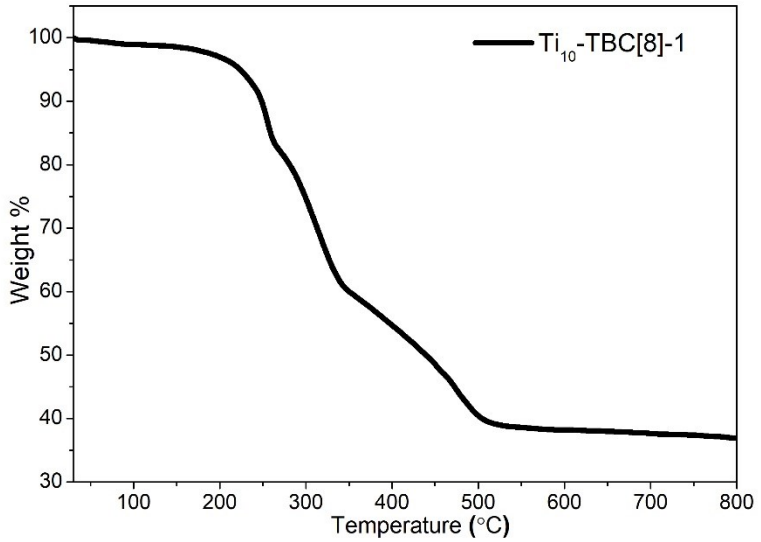

Figure S36. Thermal decomposition curve of Ti_{10}-TBC[8]-1.

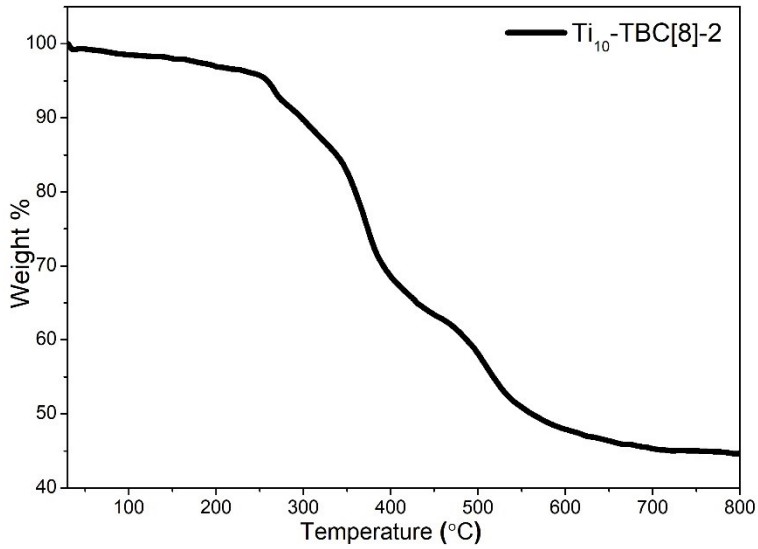

Figure S37. Thermal decomposition curve of Ti_{10}-TBC[8]-2.

5. ESI-MS measurements.

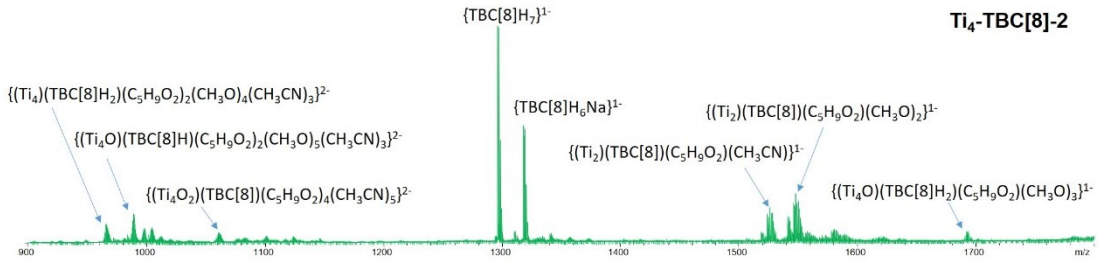

Figure S38. ESI-MS spectrum of the CH_2Cl_2/CH_3CN solution of Ti_4-TBC[8]-2.

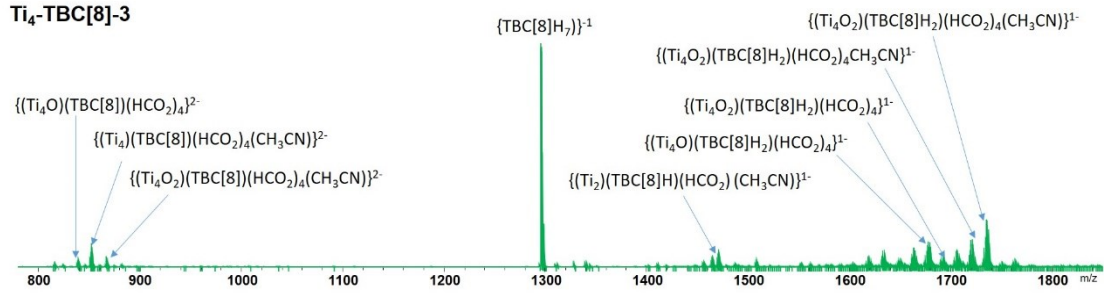

Figure S39. ESI-MS spectrum of the CH_2Cl_2/CH_3CN solution of Ti_4-TBC[8]-3.

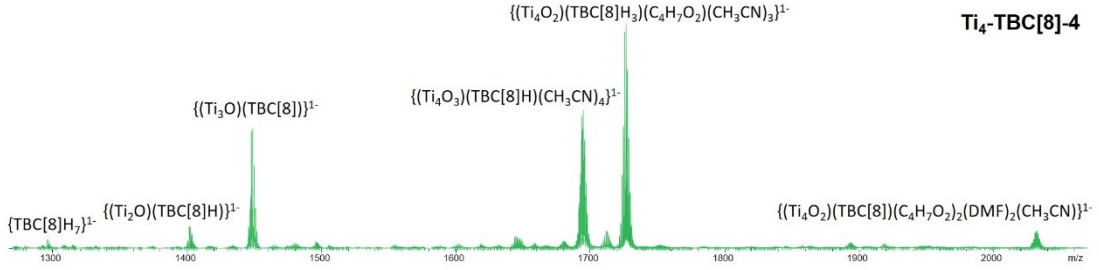

Figure S40. ESI-MS spectrum of the CH_2Cl_2/CH_3CN solution of Ti_4-TBC[8]-4.

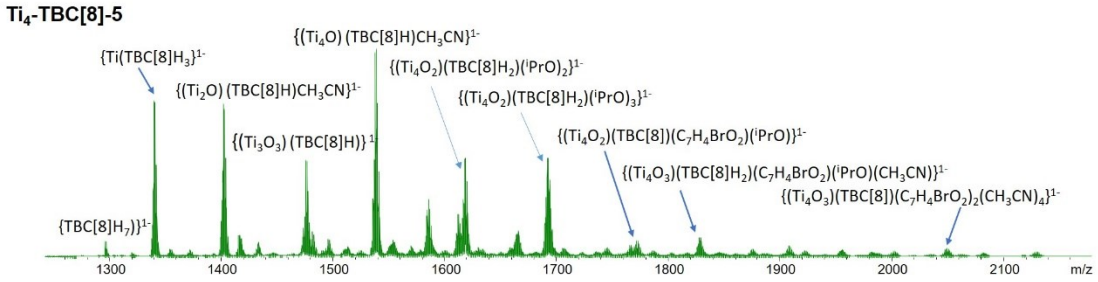

Figure S41. ESI-MS spectrum of the CH_2Cl_2/CH_3CN solution of Ti_4-TBC[8]-5.

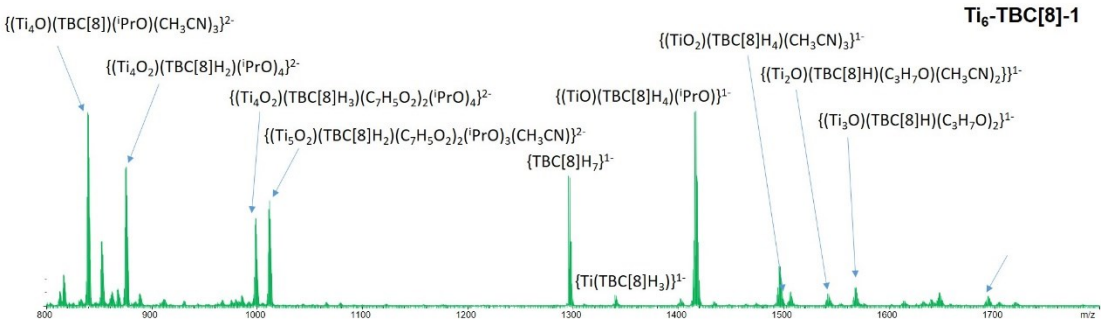

Figure S42. ESI-MS spectrum of the CH_2Cl_2/CH_3CN solution of Ti_6-TBC[8]-1.

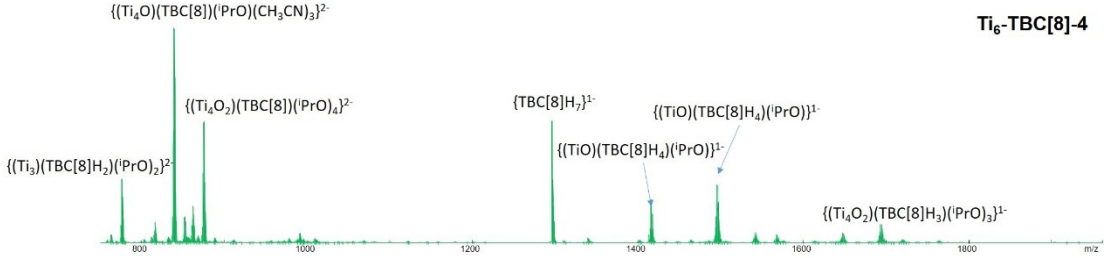

Figure S43. ESI-MS spectrum of the CH_2Cl_2/CH_3CN solution of Ti_6-TBC[8]-4.

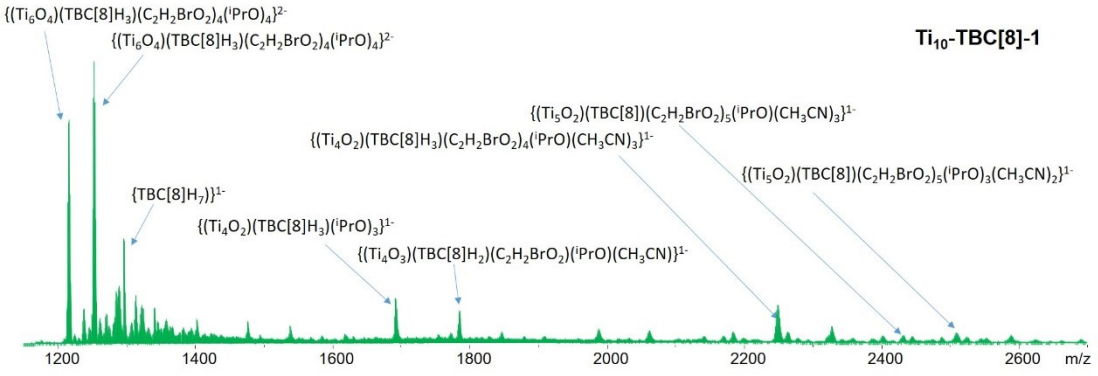

Figure S44. ESI-MS spectrum of the CH_2Cl_2/CH_3CN solution of Ti_{10}-TBC[8]-1.

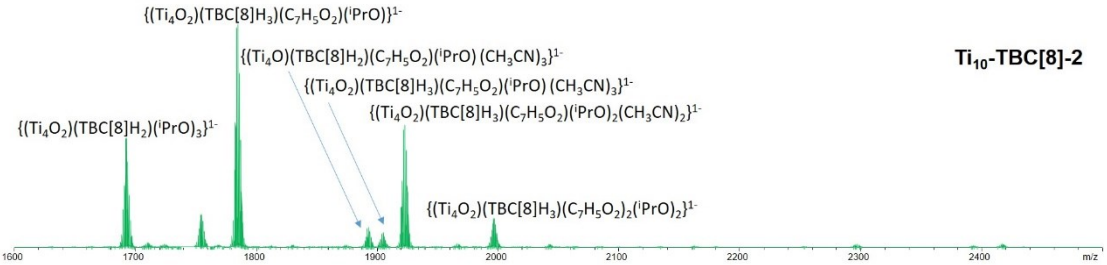

Figure S45. ESI-MS spectrum of the CH_2Cl_2/CH_3CN solution of Ti_{10}-TBC[8]-2.

5. Band-gap investigation

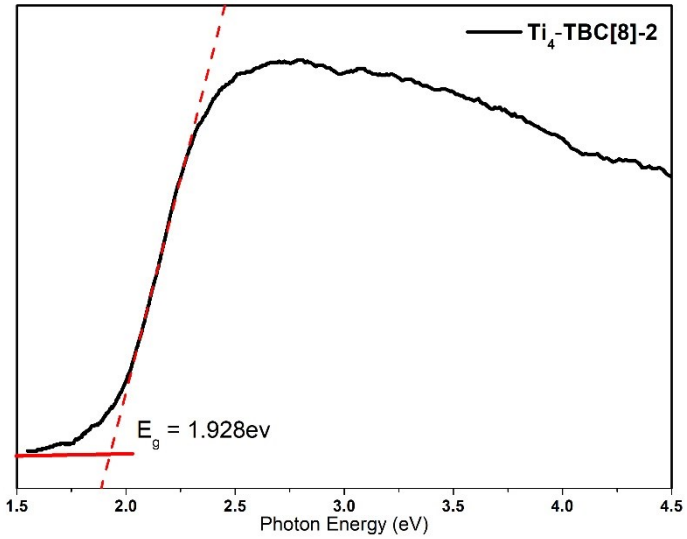

Figure 46. Kubelka–Munk transformation of diffuse reflectance data of Ti_4-TBC[8]-**2**.

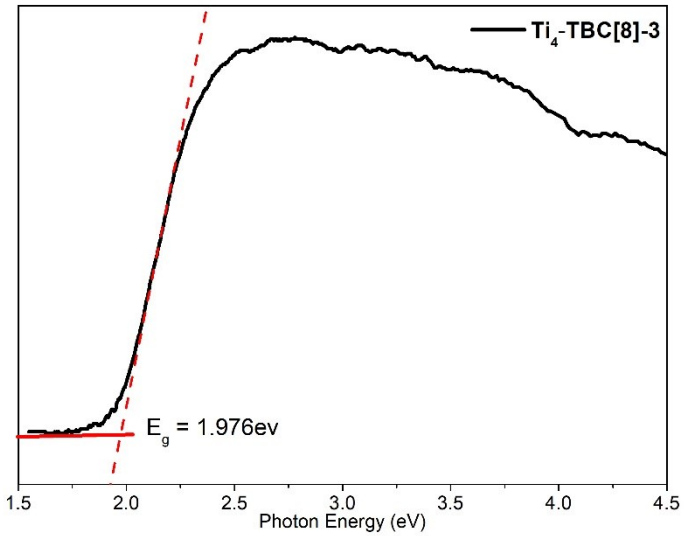

Figure 47. Kubelka–Munk transformation of diffuse reflectance data of Ti_4-TBC[8]-**3**.

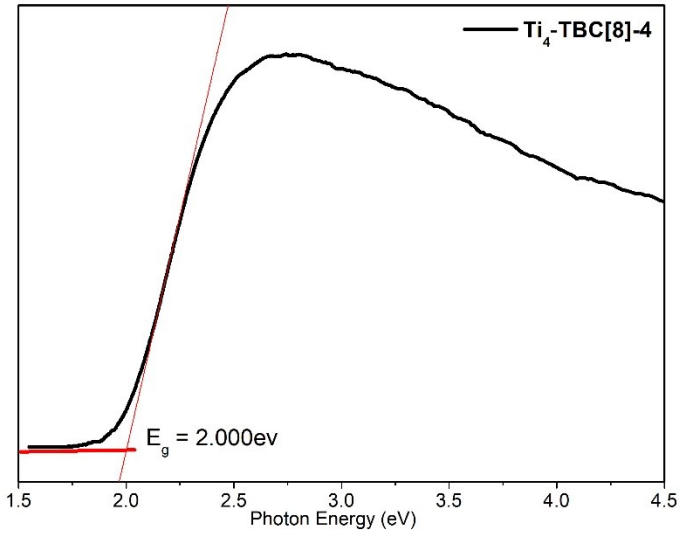

Figure S48. Kubelka–Munk transformation of diffuse reflectance data of Ti_4-TBC[8]-4

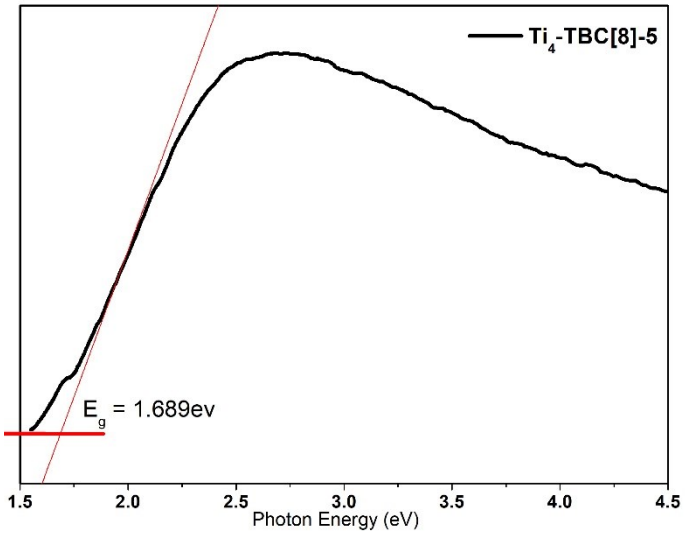

Figure S49. Kubelka–Munk transformation of diffuse reflectance data of Ti_4-TBC[8]-5.

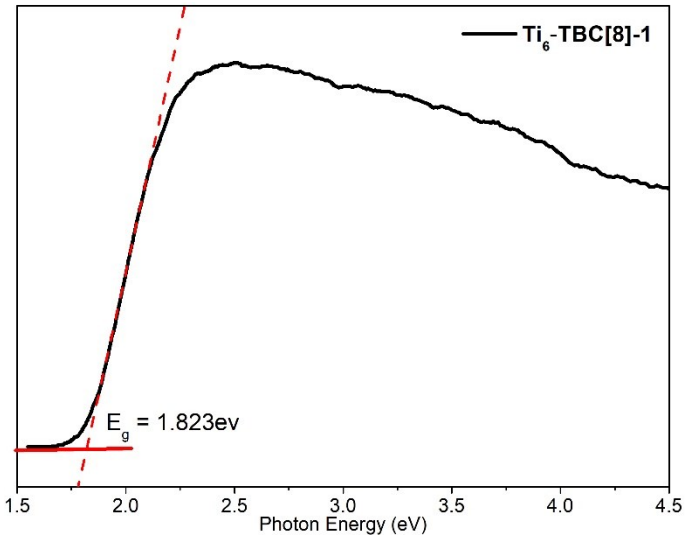

Figure S50. Kubelka–Munk transformation of diffuse reflectance data of Ti_6-TBC[8]-1.

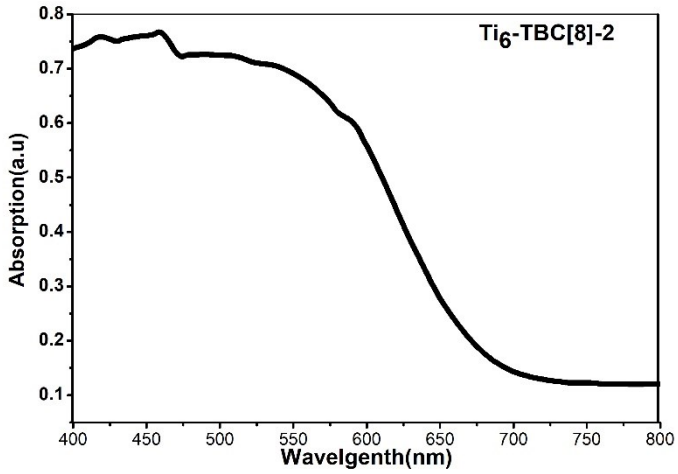

Figure S51. Solid state UV-Vis spectrum of Ti_6-TBC[8]-**2.**

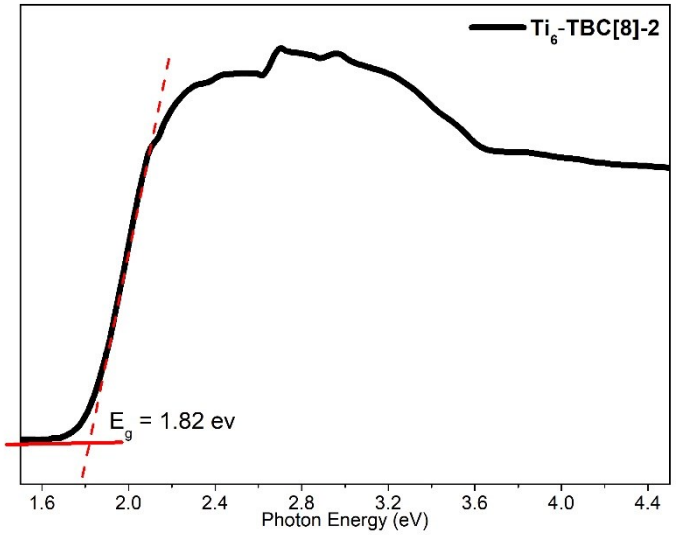

Figure S52. Kubelka–Munk transformation of diffuse reflectance data of Ti_6-TBC[8]-**2.**

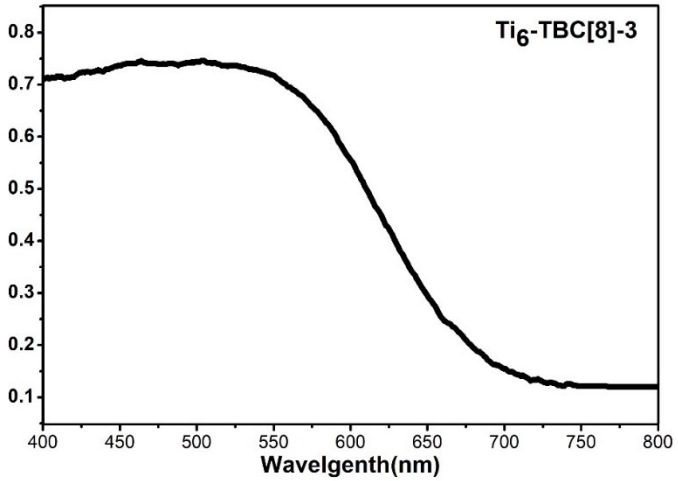

Figure S53. Solid state UV-Vis spectrum of of Ti_6-TBC[8]-**3**.

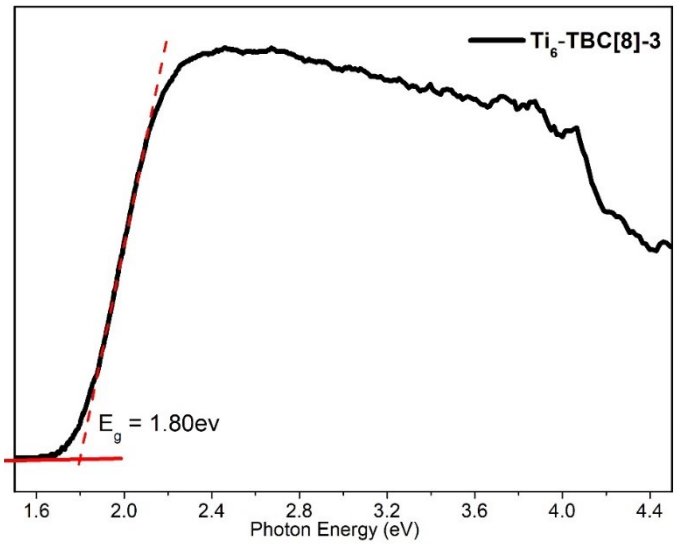

Figure S54. Kubelka–Munk transformation of diffuse reflectance data of Ti_6-TBC[8]-**3**.

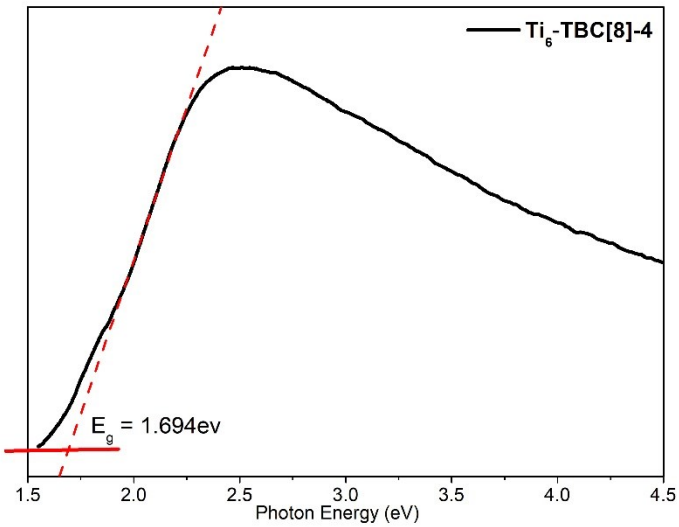

Figure S55. Kubelka–Munk transformation of diffuse reflectance data of Ti_6-TBC[8]-**4**.

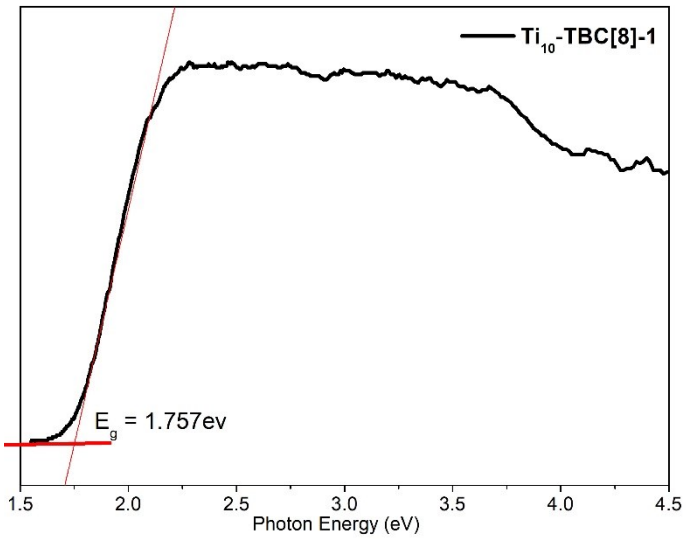

Figure S56. Kubelka–Munk transformation of diffuse reflectance data of Ti_{10}-TBC[8]-**1**.

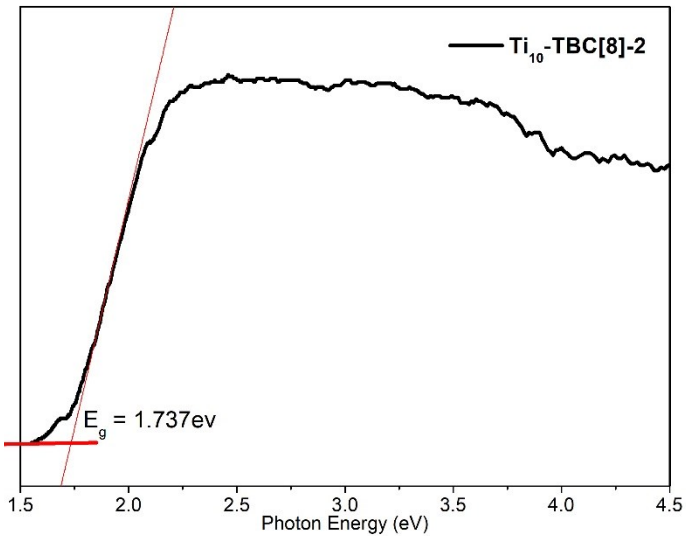

Figure S57 Kubelka–Munk transformation of diffuse reflectance data of Ti_{10}-TBC[8]-**2**.

6. Photocurrent experiments

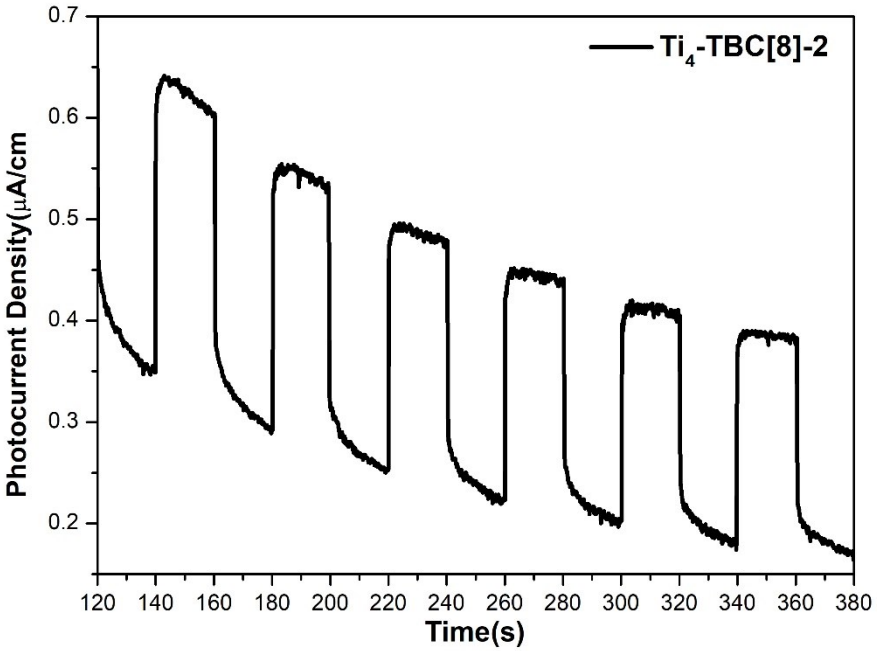

Figure S58. Photocurrent responses of Ti_4-TBC[8]-**2** in 0.2 M Na_2SO_4 aqueous solution with 0.8V (vs. NHE) bias under repetitive visible light irradiation.

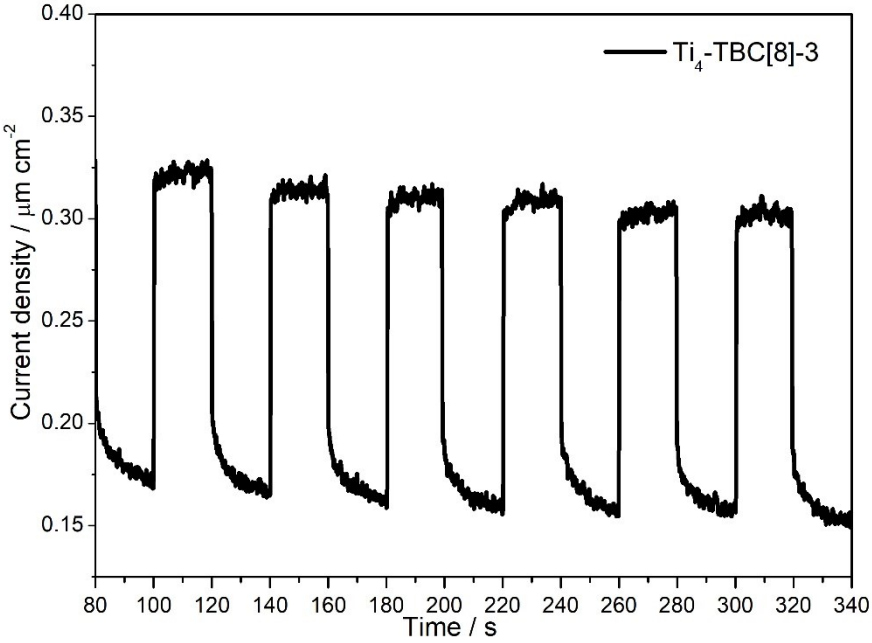

Figure S59. Photocurrent responses of Ti_4-TBC[8]-**2** in 0.2 M Na_2SO_4 aqueous solution with 0.8V (vs. NHE) bias under repetitive visible light irradiation.

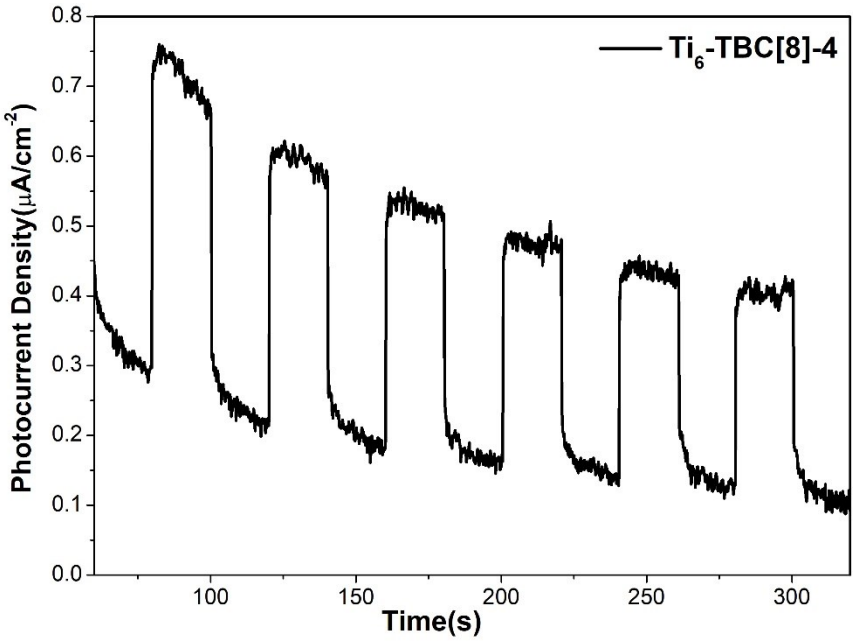

Figure S60. Photocurrent responses of Ti_6-TBC[8]-**4** in 0.2 M Na_2SO_4 aqueous solution with 0.8V (vs. NHE) bias under repetitive visible light irradiation.

7. Mott−Schottky experiments

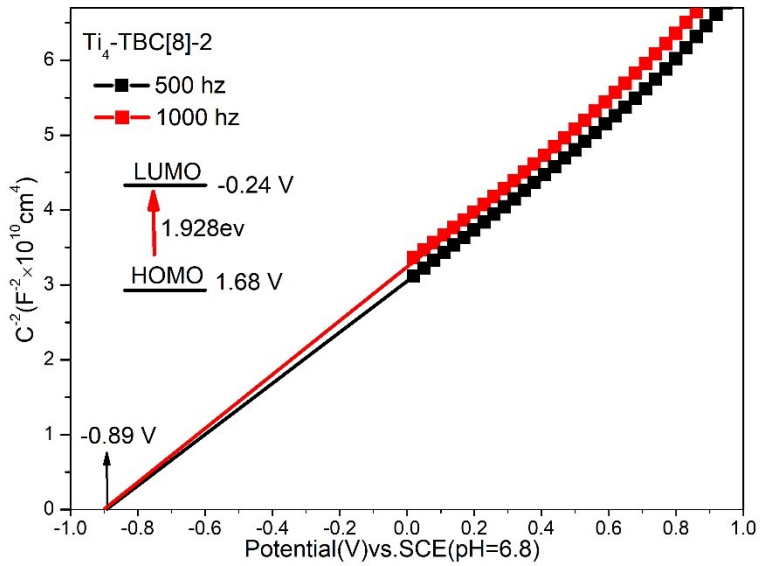

Figure S61. Mott−Schottky plots (insets are the estimated HOMO and LUMO levels of the clusters) of Ti_4-TBC[8]-**2**.

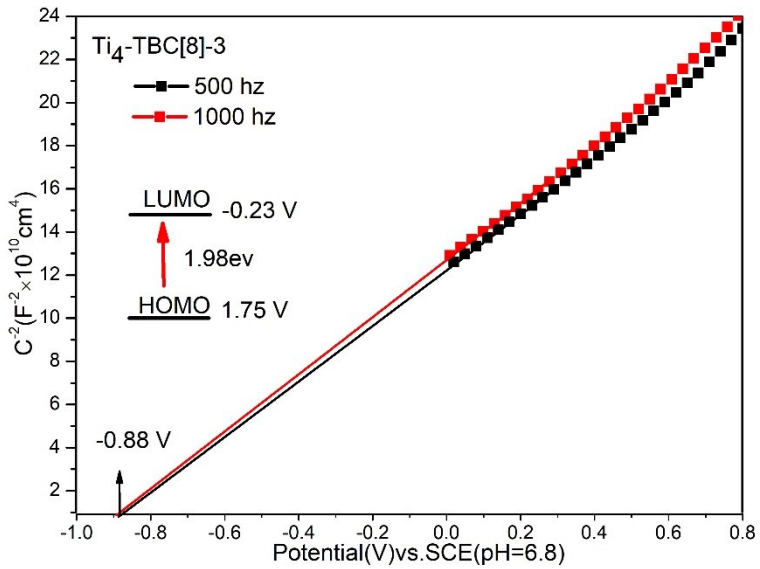

Figure S62. Mott−Schottky plots (insets are the estimated HOMO and LUMO levels of the clusters) of Ti_4-TBC[8]-**3**.

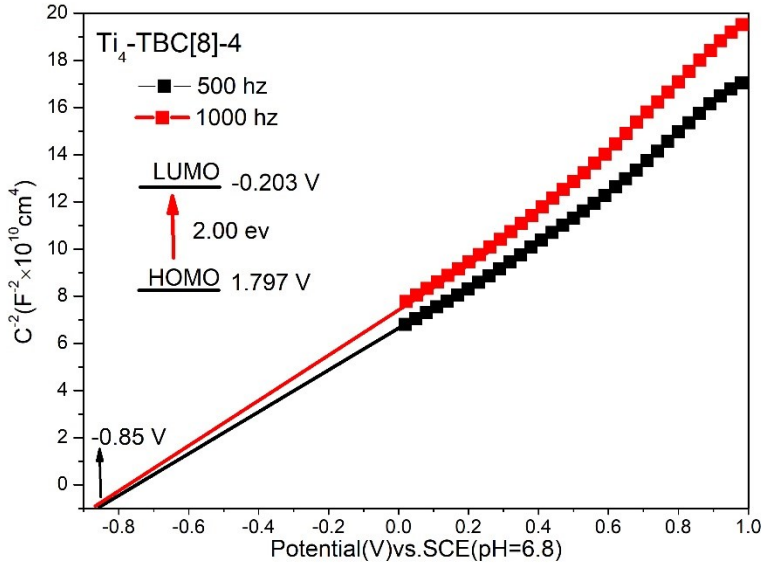

Figure S63. Mott−Schottky plots (insets are the estimated HOMO and LUMO levels of the clusters) of Ti_4-TBC[8]-**4**.

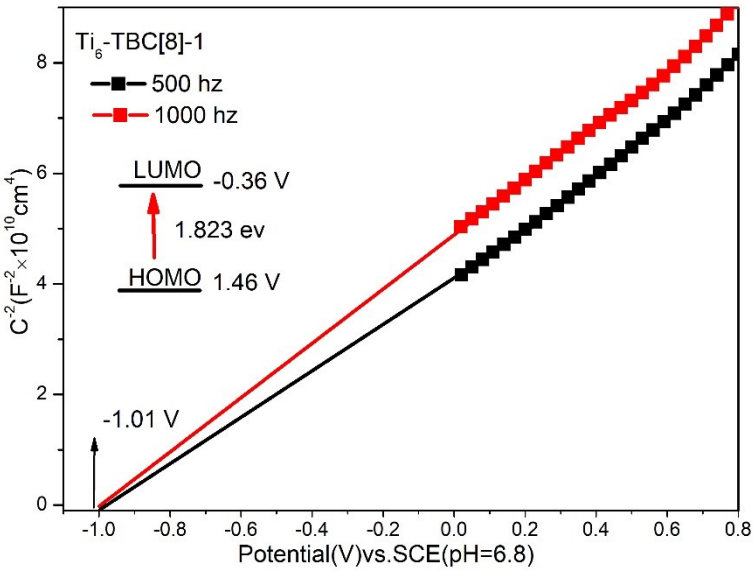

Figure S64. Mott−Schottky plots (insets are the estimated HOMO and LUMO levels of the clusters) of Ti_6-TBC[8]-**1**.

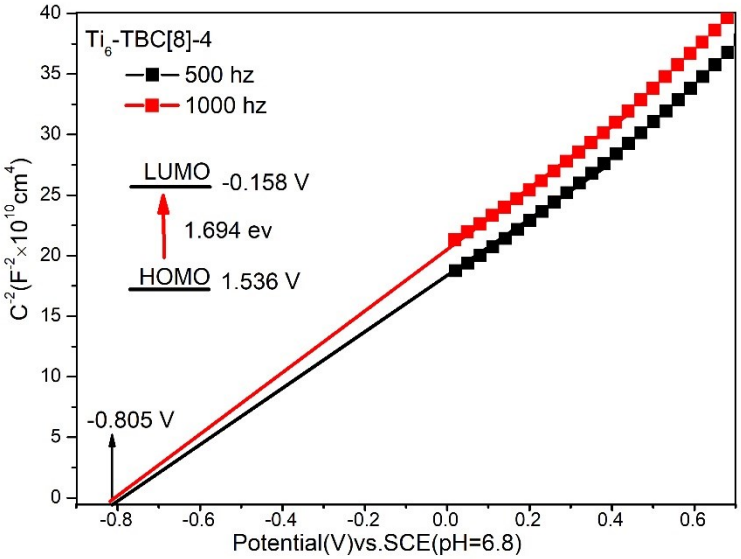

Figure S65. Mott−Schottky plots (insets are the estimated HOMO and LUMO levels of the clusters) of Ti_6-TBC[8]-**4**.

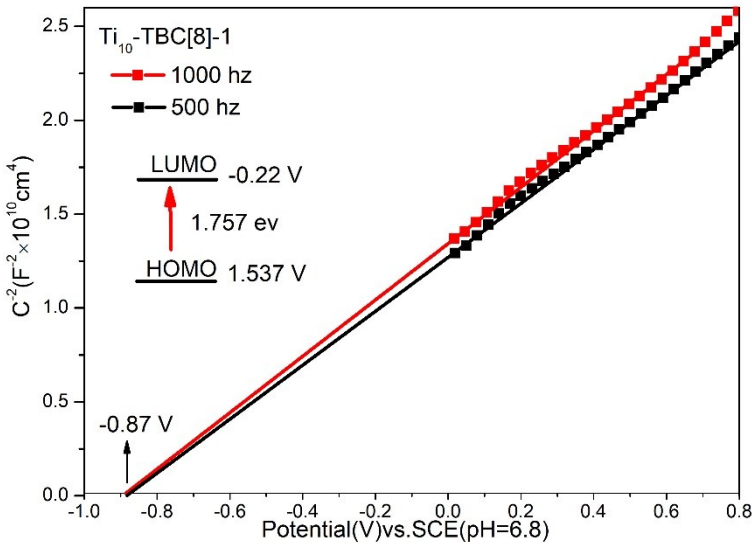

Figure S66. Mott−Schottky plots (insets are the estimated HOMO and LUMO levels of the clusters) of Ti_{10}-TBC[8]-**1**.

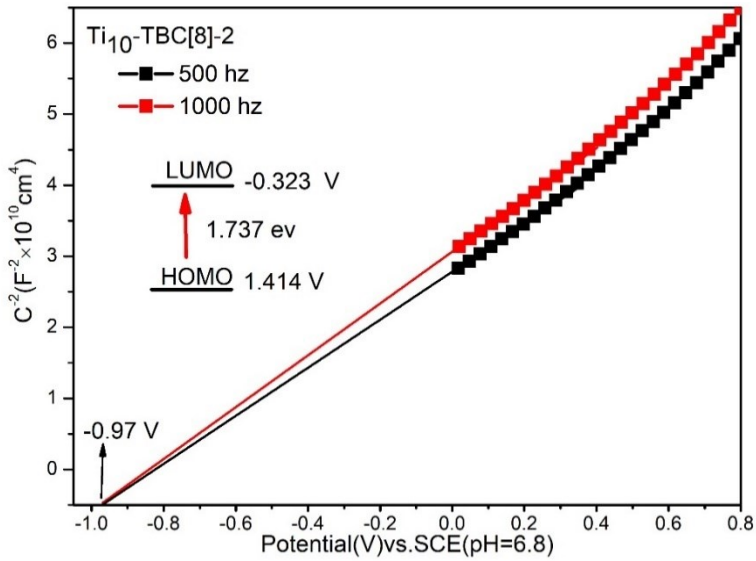

Figure S67. Mott−Schottky plots (insets are the estimated HOMO and LUMO levels of the clusters) of Ti_{10}-TBC[8]-**2**.

8. H_2 Evolution Study.

Table S2. Summary of the photocatalytic H_2 production using the Ti_x-TBC[8] as catalysts, as well as comparisons with the best TOC catalysts from the previous reports.

Complex	Co-catalyst	Sacrificial agent	H_2 production (μmol/g/h)	Ref.
Ti_4-TBC[8]-2	H_2PtCl_6	TEOA	65.88	This work
Ti_4-TBC[8]-3	H_2PtCl_6	TEOA	71.148	This work
Ti_4-TBC[8]-4	H_2PtCl_6	TEOA	67.875	This work
Ti_4-TBC[8]-5	H_2PtCl_6	TEOA	415.11	This work

Ti_6-TBC[8]-1	H_2PtCl_6	TEOA	202.14	This work
Ti_6-TBC[8]-4	H_2PtCl_6	TEOA	74.66	This work
Ti_{10}-TBC[8]-1	H_2PtCl_6	TEOA	163.04	This work
Ti_{10}-TBC[8]-2	H_2PtCl_6	TEOA	298.66	This work
Ti_{52}	H_2PtCl_6	Methanol	398	1
PTC-50 [2]	H_2PtCl_6	Methanol	267.78	2
Ti_4-TC4A	H_2PtCl_6	TEOA	252.56	3
PTC-49_V	H_2PtCl_6	Lactic acid	188	4

References:

1. A 3.6 nm Ti52−Oxo Nanocluster with Precise Atomic Structure, W. H. Fang, L. Zhang and J. Zhang, *J. Am. Chem. Soc*., 2016, ***138***, 7480–7483.
2. Synthetic investigation, structural analysis and photocatalytic study of a carboxylate–phosphonate bridged Ti18-oxo cluster, W.-H. Fang, L. Zhang and J. Zhang, *Dalton Trans*., 2017, **46**, 803–807.
3. Thiacalix[4]arene-Protected Titanium−Oxo Clusters: Influence of Ligand Conformation and Ti−S Coordination on the Visible-Light Photocatalytic Hydrogen Production, X. Wang, Y. N. Yu, Z. Wang, J. Zheng, Y. F. Bi and Z. P. Zheng, *Inorg. Chem*., 2020, **59**, 7150–7157.
4. Isomerism in Titanium-Oxo Clusters: Molecular Anatase Model with Atomic Structure and Improved Photocatalytic Activity, X. Fan, J. H. Wang, K. F. Wu, L. Zhang and J. Zhang, *Angew. Chem., Int. Ed*., 2019, **58**, 1320–1323.

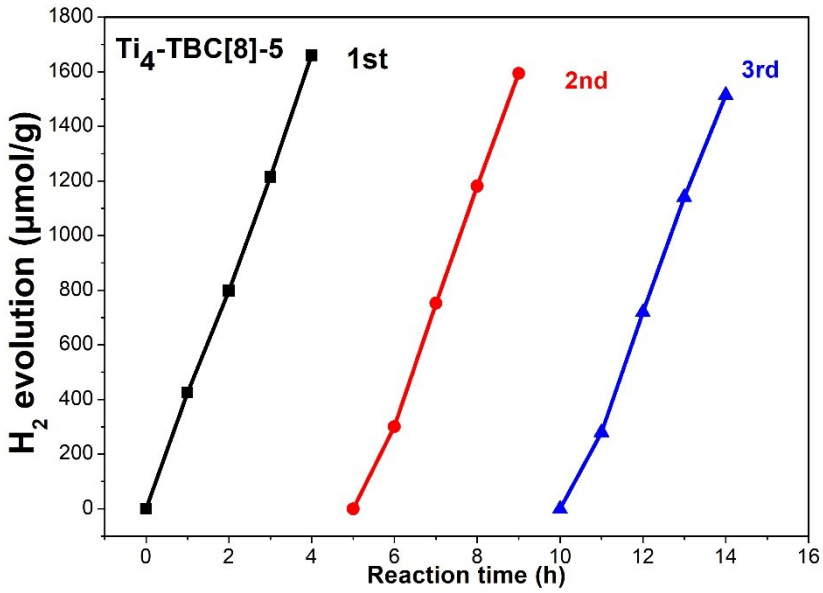

Figure S68. Recycling H_2 evolution experiments of Ti_4-TBC[8]-**5** compound.

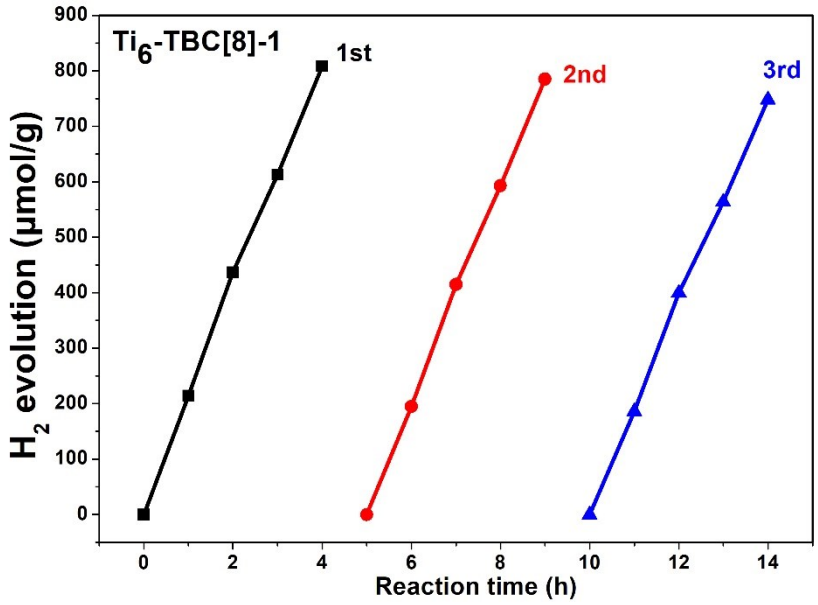

Figure S69. Recycling H_2 evolution experiments of Ti_6-TBC[8]-**1** compound.

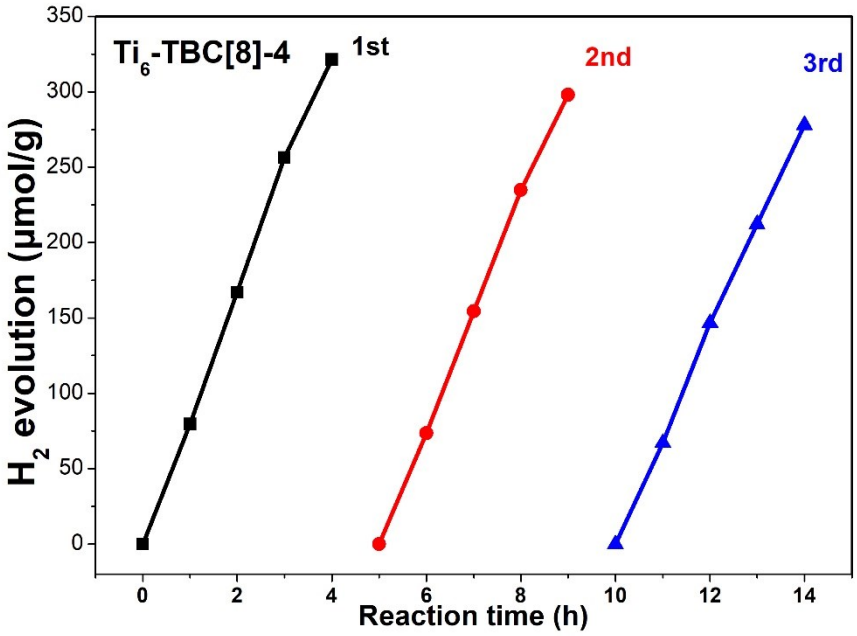

Figure S70. Recycling H_2 evolution experiments of Ti_6-TBC[8]-4 compound.

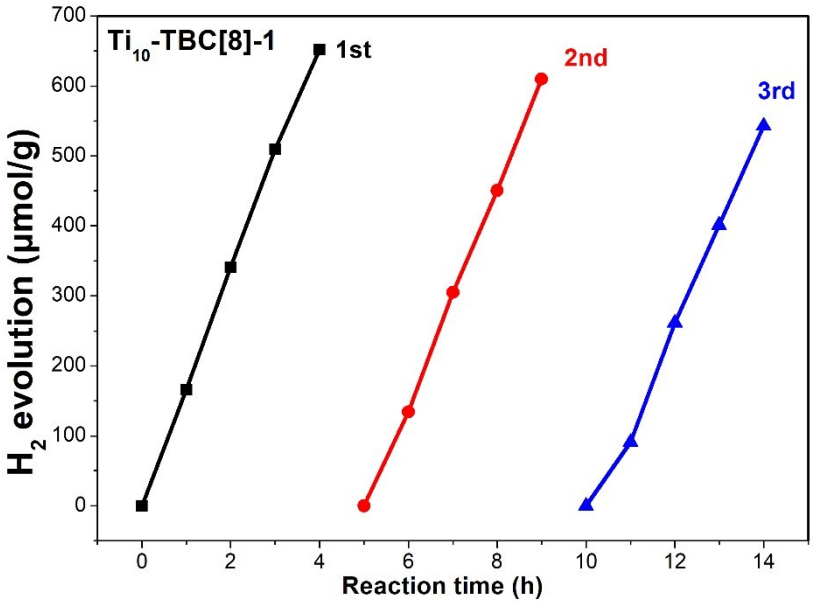

Figure S71. Recycling H_2 evolution experiments of Ti_{10}-TBC[8]-**1** compound.

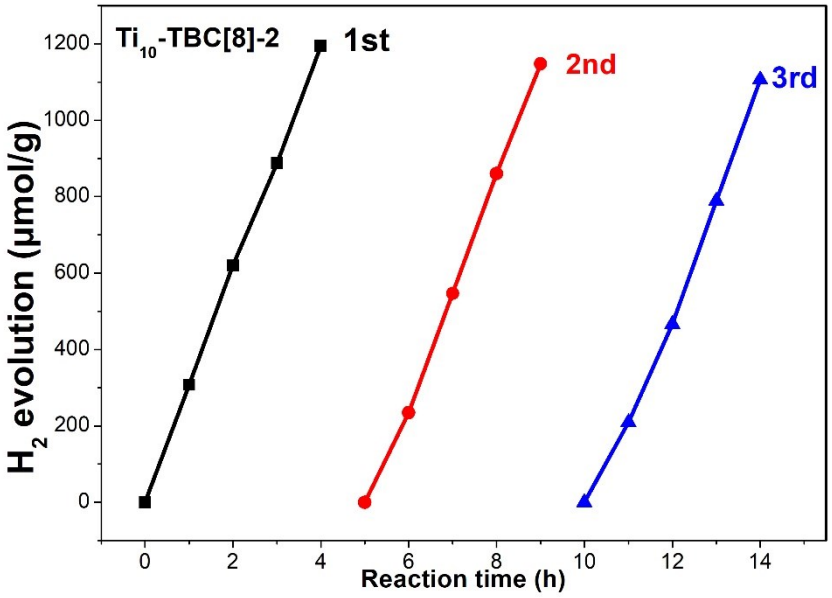

Figure S72 Recycling H_2 evolution experiments of Ti_{10}-TBC[8]-2 compound.

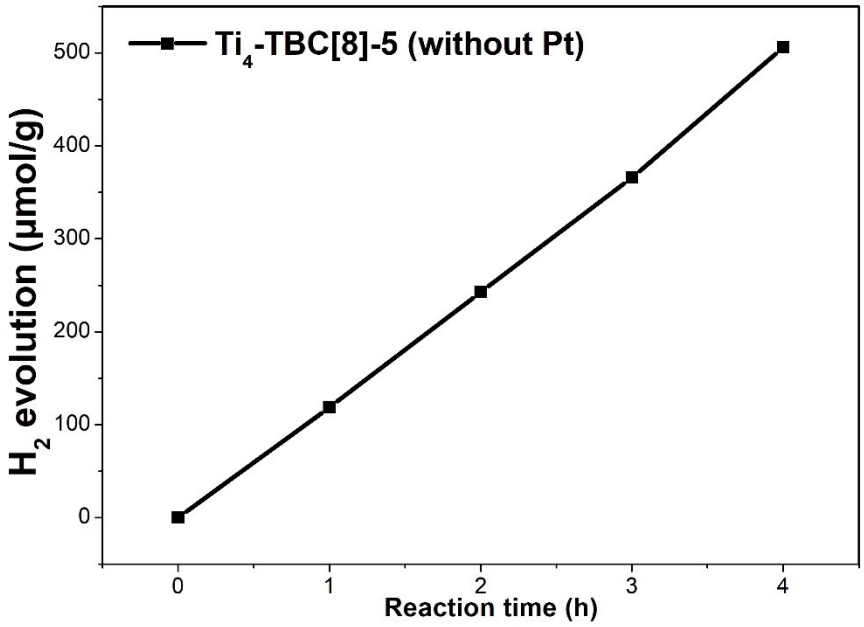

Figure S73. H_2 evolution experiment of Ti_4-TBC[8]-**5** compound without Pt co-catalyst.

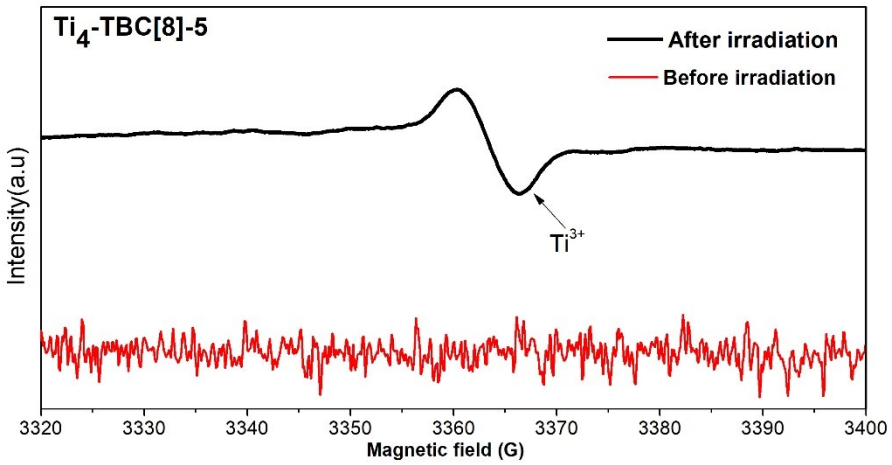

Figure S74. EPR spectra observed at 77 K for Ti_4-TBC[8]-5 before and after visible-light irradiation ($\lambda > 420$ nm).

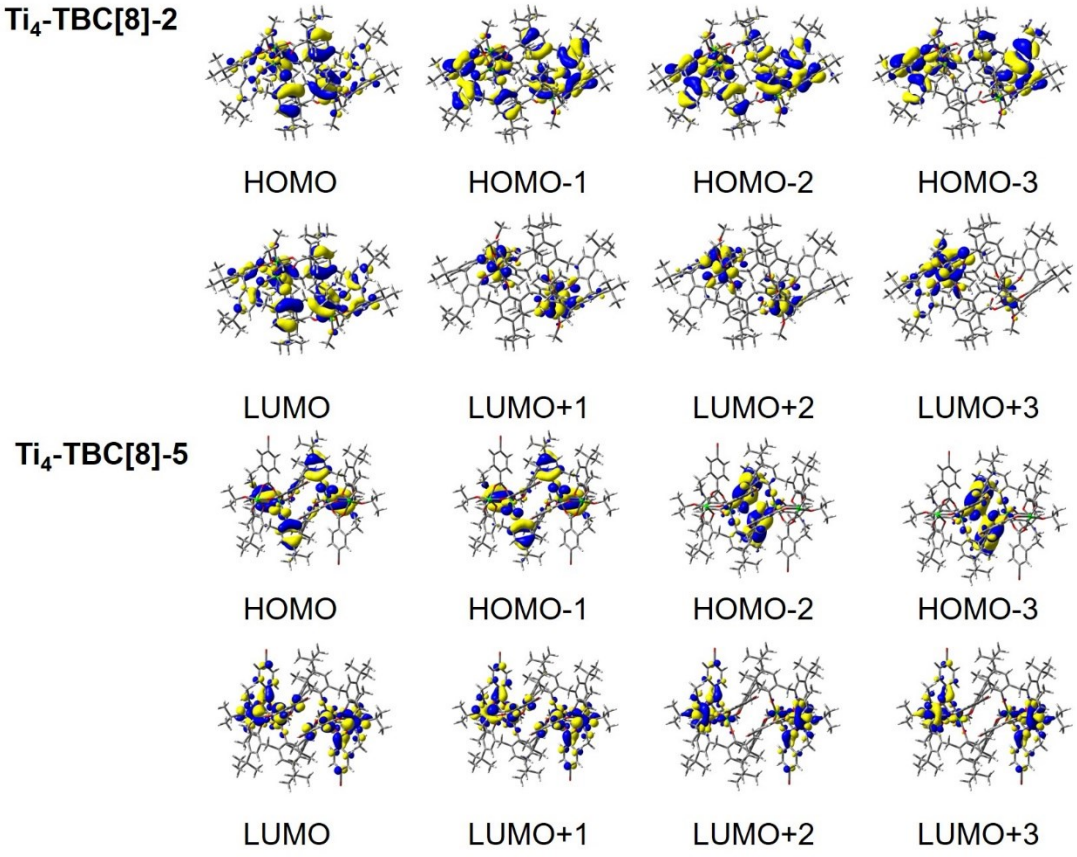

Figure S75. Some related frontier molecular orbitals of Ti_4-TBC[8]-**2** and Ti_4-TBC[8]-**5**